International Agreement Report

Analyses of an Unmitigated Station Blackout Transient in a Generic PWR-900 with ASTEC, MAAP and MELCOR Codes

Prepared by:
F. Mascari*, J. C. De La Rosa Blul**, M. Sangiorgi**, G. Bandini*

*ENEA
Via Martiri di Monte Sole 4
40129, Bologna, Italy

**European Commission JRC, Westerduinweg 3,
1755 LE Petten, The Netherlands

H. Esmaili, NRC Project Manager

Division of Systems Analysis
Office of Nuclear Regulatory Research
U.S. Nuclear Regulatory Commission
Washington, DC 20555-0001

AVAILABILITY OF REFERENCE MATERIALS
IN NRC PUBLICATIONS

International Agreement Report

Analyses of an Unmitigated Station Blackout Transient in a Generic PWR-900 with ASTEC, MAAP and MELCOR Codes

Prepared by:
F. Mascari*, J. C. De La Rosa Blul**, M. Sangiorgi**, G. Bandini*

*ENEA
Via Martiri di Monte Sole 4
40129, Bologna, Italy

** European Commission JRC, Westerduinweg 3,
1755 LE Petten, The Netherlands

ABSTRACT

The aim of the work presented in this report, jointly developed by ENEA and the European Commission JRC within the Code for European Severe Accident Management (CESAM) project funded by the 7th Framework Programme of the European Commission, is focused on the analysis of an unmitigated SBO accident in a generic Western three-loop PWR 900 MWe, until RPV failure, with MAAP 5.02 and MELCOR 2.1 code to benchmark ASTEC 2.1 code, in the field of severe accident sequence application, considering selected figures of merit as a basis for comparison. The main thermal-hydraulic and in-vessel degradation phenomena, as simulated by the three severe accident codes, have been analyzed. A detailed quantitative analysis of the core energy balance, of the core degradation and relocation, corium physical and chemical composition together with the influence played by natural circulation flows between the core, upper plenum and steam generators predicted by the three codes is not presented here but it is planned for future research activity.

FOREWORD

After the Fukushima accident, the interest of each country using nuclear energy as a part of its national energy mix has been more focused on severe accident mitigation strategies. Within this regard, the use of best estimate state-of-the-art severe accident code can be considered the best approach to design a suitable accident management strategy, permitting the phenomenological analyses of the main severe accident phenomena characterizing the Reactor Pressure Vessel (RPV), the Reactor Cavity (RC), the Containment, and the confinement buildings typical of LWRs. Among the accidents usually considered in the field of BDBA leading to core damage, an unmitigated Station Blackout (SBO) without crediting to any kind of safety not mitigating system is currently of great interest in the International Scientific Community.

In the framework of the European Project CESAM (Code for European Severe Accident Management), coordinated by GRS, in the WP40 - Plant applications and Severe Accident Management (SAM)-, coordinated by JRC, ENEA has been involved in the development of a "Generic PWR 900" with MELCOR code for benchmarking ASTEC code. Within this regard, ENEA and JRC started a joint research activity focused on the analysis of an unmitigated Station Blackout (SBO) with MELCOR (analyses performed by ENEA) and MAAP (analyses performed by JRC) codes to benchmark ASTEC code (analyses developed by JRC). In this report the results of the benchmark have been revised and presented considering selected figures of merits.

TABLE OF CONTENTS

LIST OF FIGURES

LIST OF TABLES

EXECUTIVE SUMMARY

In the framework of the European Project CESAM (Code for European Severe Accident Management), in the WP40 - Plant applications and Severe Accident Management (SAM)- ENEA has been involved in the development of a "Generic PWR 900" with MELCOR code for benchmarking ASTEC code. Within this regard, ENEA and JRC started a joint research activity focused on the analysis of an unmitigated Station Blackout (SBO), until RPV failure, with MELCOR and MAAP codes to benchmark ASTEC code (analyses developed by JRC). The main thermal-hydraulic and in-vessel degradation phenomena, as simulated by three severe accident system codes, have been investigated. The reference reactor is a 900 MWe, generic Western three-loop PWR. The postulated accident is characterized by the loss of offsite Alternating Current (AC) power and the concurrent failure of the emergency diesel generator determining that active safety injection systems are unavailable. These hypotheses are coupled with the unavailability of the accumulator, no leakage through the Main Reactor Coolant Pump (RCP) seals, and SCRAM, pump coast-down and SG isolation at the Start of the Transient (SOT). The only credited human action within the post-core damage strategy consists of depressurizing the primary system by opening the pressurizer SEBIM valves.

ASTEC, MAAP and MELCOR reference NPP nodalizations have been developed starting from the same generic PWR 900 three loops model delivered by IRSN during the EU-CESAM project. The target of this exercise is to analyze, considering the code modelling differences, the main transient phenomena through the selection of some safety related figure of merits. This allows, by assuming a geometrically congruent code nodalization (as much as possible considering the geometrical plant data available, the code nodalization topology characteristics and nodalization user guidelines typical of each code) and consistent boundary and initial conditions, to compare and discuss the results of the code calculations. The consequent discussion of the calculated data and the analysis of the predicted phenomena give the possibility to understand if the different code predictions are consistent and give comparable results. This allows confirmation of the transient phenomenology and the time sequence of the main accident safety relevant aspects. Since the target of the CESAM project is related to the improvement of ASTEC severe accident analysis capability, the discrepancies between ASTEC and MAAP/MELCOR calculated data are reported and analyzed considering some figure of merits as a basis for comparison.

A steady state analysis, at the same reactor operational point, has been performed to analyze the different code steady state conditions congruence before starting the comparison of the SBO transient calculated data. After reaching stable and comparable steady state conditions, the Start of the Transient (SOT) takes place. The thermal-hydraulic and the core degradation phases, until RPV failure, have been simulated by the three codes. The analysis and discussion of the code results has been developed considering three different phases:

o A first phase starting from the initiating event until core heat-up; this phase is dominated by thermal-hydraulic phenomena;
o A second phase starting from the core heat-up phase until the core relocation in the lower plenum; this phase is dominated by core degradation phenomena;
o A third phase, starting from the core relocation in the lower plenum until the vessel failure; this phase is also dominated by core degradation phenomena.

The results of the calculated data show that the three codes predict the phenomenological evolution in a good qualitative agreement with some quantitative differences. Considering the time sequence of relevant phenomenological aspects, the maximum percentage discrepancy between ASTEC and MAAP/MELCOR calculated data is about 20% for the main selected safety related parameters chosen as figure of merit. The most relevant differences are observed in the in-vessel hydrogen mass production prediction. Such discrepancies underline some modeling differences between the three codes related to core material degradation/relocation, determining differences in the available area for the oxidation process, different flow blockage conditions, different core node porosity prediction, etc. It is important to underline that the area available for the oxidation has a great uncertainty due to the complex phenomena taking place during the degradation and relocation of the core material and the limited full-scale experimental data for validation purpose. In addition, a phenomenological discrepancy related to the slumping predictions between ASTEC and MAAP/MELCOR calculations should be highlighted. While, in this case, MAAP and MELCOR predict a core lower plate failure with a consequent relocation of degraded core material in the lower plenum, ASTEC, in this case, predicts the relocation of the degraded core material through the shroud failure. In the ASTEC calculation, hydrogen is produced before the core relocation to the lower plenum, while in the MAAP and MELCOR calculations, hydrogen is also produced during this phase.

A detailed quantitative analysis of the core energy balance (decay energy in the core, oxidation energy, stored energy in the core, radiative heat loss, convective heat loss), core degradation and relocation, corium physical and chemical composition together with the influence played by natural circulation flows between the core, upper plenum and steam generators predicted by the three codes is not presented here but may be considered for further research. This activity, in collaboration with the code developers could be the basis for a future PWR "crosswalk activity" to investigate the code calculated data differences through the identification of the principal modelling capability of each code and user effect. Future activities based on a strictly congruence analysis between core structure nodalizations (geometry and mass) are recommended.

ACKNOWLEDGMENTS

ABBREVIATIONS AND ACRONYMS

AC	Alternating Current
AFW	Auxiliary Feed Water
ASTEC	Accident Source Term Evaluation Code
BAF	Bottom of Active Fuel
BWR	Boiling Water Reactors
BP	Bypass
CAV	Cavity
CET	Core Exit Temperature
BDBA	Beyond Design Basis Accident
CESAM	Code for European Severe Accident Management
CL	Cold Leg
CVH	Control Volume Hydrodynamics
COR	Core Behavior
DBA	Design Basis Accident
DC	Downcomer
DCH	Direct Containment Heating
DISCR	DISCRepancy
ECCS	Emergency Core Cooling System
EFWS	Emergency Feedwater System
ENEA	Agenzia nazionale per le nuove tecnologie, l'energia e lo sviluppo economico sostenibile
EPRI	Electric Power Research Institute
ESF	Engineered Safety Features
FL	Flow Paths
FW	Feed Water
GRS	Gesellschaft für Anlagen- und Reaktorsicherheit (GRS) gGmbH
HL	Hot Leg
HPIS	High Pressure Injection System
HPME	High Pressure Melt Ejection
HS	Heat Structure
IRSN	Institut de radioprotection et de surete Nucleaire (Institut for radiological Protection and Nuclear Safety)
JRC	Joint Research Centre
LH	Lower Head
LP	Lower Plenum
LPIS	Low Pressure Injection System
LWR	Light Water Reactor
MAAP	Modular Accident Analysis Program
MELCOR	Methods of Estimation of Leakages and Consequences of Releases
MDAFW	Motor-driven Auxiliary Feedwater
MFW	Main Feed Water
MSL	Main Steam Line
NPP	Nuclear Power Plant
NRC	Nuclear Regulatory Commission
PCV	Primary Containment Vessel
PORV	Pilot-Operated Relief Valve
PRZ	Pressurizer
PWR	Pressurized Water Reactor

RC	Reactor Cavity
RCP	Reactor Coolant Pump
RN	RadioNuclide
RPV	Reactor Pressure Vessel
RPS	Reactor Protection System
SBO	Station Black-Out
SCRAM	Safety Control Rod Axe Man
SEBIM	Safety Valves of Pressure Compensator
SG	Steam Generator
SGTR	Steam Generator Tube Rupture
SNAP	Symbolic Nuclear Analysis Package
SL	Steam Line
SNL	Sandia National Laboratories
SOT	Start Of the Transient
SRV	Safety Relief Valve
TAF	Top of Active Fuel
TDAFW	Turbine Driven Auxiliary Feedwater
UH	Upper Head
UP	Upper Plenum
USNRC	US Nuclear Regulatory Commission
UT	U-Tube

1 INTRODUCTION

After the Fukushima accident, the interest of each country using nuclear energy as a part of its national energy mix has been more focused on severe accident [1-7] mitigation strategies. Several severe accident management analyses have been performed to analyze the accident progression, the core damage, the grace period and the fission product release demonstrating the accident management strategy adequacy.

Nuclear reactors are designed to maintain the fuel damage and radioactive release within authorized limits during selected postulated accident - Design Basis Accident (DBA) -. A severe accident is a Beyond Design Basis Accident (BDBA) involving significant core degradation. Several computational tools can be used to analyze a severe accident. Considering the complexity and mutual different interacting and interrelated phenomena/processes along a severe accident transient progression, a key role is played by the state-of-the-art severe accident integral codes [14] such as ASTEC [8,9], MAAP [10,11], and MELCOR [12,13] that can be considered the key tool to design a suitable accident management strategy.

These codes, storing all the knowledge developed in the last decades from the experimental activities, allow confirmation of the transient progression of the modeled plant, during a postulated severe accident, characterizing the main severe accident phenomena taking place in the Reactor Pressure Vessel (RPV), the Reactor Cavity (RC), the Containment (PCV), and the confinement buildings typical of LWRs. Several models/correlations have been implemented in these state-of-the-art severe accident codes and must be set by the code user during input deck development.

Several experimental programs in the field of severe accident phenomena [15-19] have been conducted to validate the models and correlations implemented in the codes and provided a valuable "assessment database [20]" to assess severe accident simulation tools. However, the analyses of the current state-of-the-art shows that there is a need to reduce some uncertainties still present [21] and a consequent investigation of phenomena/processes, to date not investigated in detail in geometric prototypical experimental facility with prototypical material, should be addressed. Therefore, discrepancies in some core degradation phenomena can be still observed when comparing the results as predicted by different simulation tools considering the different core degradation models implemented in the codes [22].

Within this framework, code-to-code exercises called "crosswalk" activities involving the teams of code developers have been performed and must be continued to identify the modelling differences affecting code prediction results. Examples are the MAAP/MELCOR crosswalk reported in [23,24] and the ASTEC/MELCOR crosswalk reported in [25].

In relation to the user-effect [26,27], considering the several complex and different phenomena/processes taking place during a severe accident, code-users require a high-level understanding of the phenomena/processes and need to define several modelling parameters in the use of a severe accident code. To contribute to such efforts, a code-to-code benchmark exercise, as an independent user crosswalk activity can also give some insight and characterize the influence of user effect on the different code predictions. An example of independent user cross walk activity developed during the EU-CESAM project [28,29] and presented in [4, 30], is extensively investigated in this report.

Among the accidents usually considered in the field of Beyond Design Basis Accident (BDBA) leading to core damage, an unmitigated Station Blackout (SBO) accident [31] is currently of great interest in the International Scientific Community.

The aim of this work, developed within the Code for the European Severe Accident Management (CESAM) [32] project funded by the 7th Framework Programme of the European Commission, is a benchmark exercise to study an unmitigated SBO accident, until RPV failure, where the main thermal-hydraulic and in-vessel degradation phenomena, as simulated by three severe accident system codes ASTEC 2.1, MAAP 5.02 and MELCOR 2.1, have been analyzed. The reference reactor is a 900 MWe, generic Western three-loop PWR. The postulated accident is characterized by the loss of offsite Alternating Current (AC) power and the concurrent failure of the emergency diesel generator determining that active safety injection systems are unavailable. These hypotheses are coupled with the unavailability of the accumulator, no leakage through the Main Reactor Coolant Pump (RCP) seals, and SCRAM, pump coast-down and SG isolation at the Start of the Transient (SOT). The only credited human action within the post-core damage strategy consists of depressurizing the primary system by opening the pressurizer SEBIM valves.

ASTEC, MAAP and MELCOR reference NPP nodalizations have been developed starting from the same generic PWR 900 three loops model delivered by IRSN during the CESAM project [33,34]. The target of this exercise is to analyze, considering the code modelling differences, the main transient phenomena through the selection of some safety related figure of merits. This allows by assuming a geometrically congruent code nodalization (as much as possible considering the geometrical plant data available, the code nodalization topology characteristics and nodalization user guidelines typical of each code) and consistent boundary and initial conditions, to compare and discuss the results of the code calculations. The consequent discussion of the calculated data and the analysis of the predicted phenomena give the possibility to understand if the different code predictions are consistent and give comparable results. This allows confirmation of the transient phenomenology and the time sequence of the main accident safety relevant aspects. Since the target of the CESAM project is related to the improvement of ASTEC severe accident analysis capability, the discrepancies between ASTEC and MAAP/MELCOR calculated data are reported and analyzed considering some figure of merits as a basis for comparison.

This analysis is focused mainly on the characterization of main relevant thermal hydraulics and core degradation safety aspects considering selected main macroscopic safety parameters as a figure of merit for the comparison (primary pressure, fuel cladding temperatures, hydrogen production, inception of the core ring failure, core plate failure, and lower head failure). A detailed analysis and characterization of the core degradation/relocation evolution and morphologies, predicted by the three codes, is not presented here but it is recommended for further research activity. The current analysis also attempts to provide clear rationale underlying significant discrepancies among the depicted code results whenever found. This activity, in collaboration with the code developer teams, could be the basis for future PWR "crosswalk activity" to investigate the code calculated differences through the identification of the principal modelling capability of each code and the user effect.

2 SBO TRANSIENT MAIN CHARACTERISTICS

The SBO transient is considered unmitigated and the initiating event is a loss of offsite Alternating Current (AC) power with a failure of all the diesel generators. This determines that Pressurizer (PRZ) level control, RCP seal injection, active safety injection systems (HPIS and LPIS), Motor-driven Auxiliary Feedwater (MDAFW) system are unavailable. Further the following hypotheses are also considered:

a) Independent failure of the Turbine Driven Auxiliary Feedwater (TDAFW) pump (no AFW available);
b) No RCP seal failure,
c) Independent failure of the accumulators;
d) No primary boundary structures thermal induced degradation phenomena (SGTR not considered, HL/surge line creep rupture not considered);
e) Primary and secondary side relief valves availability throughout the accident evolution;
f) Post core damage strategy is assumed (SEBIM manually stuck open when the core exit temperature CET reaches 650 °C).

The Loss of offsite Alternating Current (AC) power determines the reactor trip and the consequent isolation of the SGs via the MFW and MSL isolation. This first phenomenological window is characterized by the role of the SG as the only primary side heat sink. Considering that the RCP failure is not considered, its small contribution to removal of the core residual heat is not present. Another small contribution to the core residual heat removal mechanism is the heat loss of the primary system to the containment. The secondary side pressure starts to increase, due to the energy removed from the primary side and, when the secondary side opening pressure set points are reached, the relief valves start to operate causing a pressure oscillation and a decrease of the secondary side water inventory. The primary system is characterized by a single-phase natural circulation that is sustained, for a short time after the scram, by pump coast-down. A primary pressure decrease takes place and a quasi-steady state condition could be obtained during the SG relief cycling phase till the secondary side inventory is able to remove the core residual heat.

As the secondary side inventory decreases, its capability to act as heat sink becomes less efficient until reaching water depletion and leading to a primary pressure increase which is limited by the opening of the SEBIM valves causing a continuous loss of the primary system inventory.

The TAF (Top of Active Fuel) will start to uncover and the fuel will heat-up with a consequent oxidation reaction between the steam and the fuel rod cladding; as a result, oxidation heat generation will add to fission product decay heat producing hot steam in the core which will release energy from the core to the primary pressure boundary structures due to natural circulation. Steam production in the core determines a heat transfer decrease between the fuel rods and the primary coolant determining in turn an increase of the fuel temperature. Hydrogen starts to be generated due to the metal-water oxidation reaction that takes place on the exterior surface of the fuel rod cladding. Because of the core temperature excursion, the CET reaches 650 °C and the SEBIM are manually stuck open.

Along the core degradation and melt progression phase, the cladding and fuel failure mechanism and the consequent core materials transport and relocation take place with a consequent loss of core geometry. After core material relocation into the lower plenum,

additional hydrogen could be generated due to the oxidation phenomena. After the core slumping, all the liquid water present in the lower plenum evaporates due to the relocation of the degraded core material; this causes an increase of the RCS pressure, as a short-term effect.

The long-term phenomenological behavior is dominated by the physical and chemical phenomena and lower plenum boundary conditions which in turn determines the timing of the lower head failure.

3 CODE DESCRIPTION

3.1 ASTEC

The ASTEC code [8,9] (Accident Source Term Evaluation Code), jointly developed until 2015 by the French "Institut de Radioprotection et de Sûreté Nucléaire" (IRSN) and the German "Gesellschaft für Anlagen und Reaktorsicherheit mbH" (GRS), and developed now only by IRSN, aims at simulating an entire Severe Accident (SA) sequence in nuclear water-cooled reactors from the initiating event through the release of radioactive elements out of the containment. ASTEC includes several coupled modules that can deal with the different severe accident phenomena: thermal-hydraulics in the reactor system, core degradation and melt release, fission product release and transport, ex-vessel corium interaction, aerosols behavior and iodine chemistry in the containment, etc. Therefore, ASTEC is mainly used for estimating the source term following a SA, but also for level 2 Probabilistic Safety Assessment (PSA2) studies, the effectiveness of SA Management (SAM) measures, or the analysis of experiments.

ASTEC progressively became the reference European severe accident integral code for water-cooled reactors through new knowledge acquired in the frame of the SARNET European Network of Excellence from 2004 to 2013 [35,37].

ASTEC is constituted by modules which can work as stand-alone or coupled to each other's, where each module simulates a reactor zone or a set of physical phenomena.

3.2 MAAP

The Modular Accident Analysis Program (MAAP) [10,11] is an integral system code aimed at calculating the accident evolution from the initiating event up to the radiological releases to the outside environment.

MAAP code has been tailored for different light water reactor designs including different types of Western Pressurized Water Reactors, Boiling Water Reactors and Heavy Water Reactors based on Canadian design (CANDU reactors). Its latest versions also allow the modelling of some of the advanced reactor designs such as the AP1000.

Given a set of initiating events and operator actions, MAAP predicts the plant response in a relatively fast calculation as the accident progresses. MAAP results are used world-wide to determine Level 2 PRA Release Categories and accident timing to support human reliability analyses and in-plant design modifications. The code is used for the following main applications:

- Prediction of main figures of merit dealing with the severe accident;
- Verification of accident management actions;
- Characterization of radioactive releases in time, magnitude and composition;
- To calculate in-plant and ex-plant dose in a single run (only MAAP5);
- Integration in full-scope simulators with the capability of severe accidents.

Among the severe accident spectrum of phenomena, MAAP capabilities include clad ballooning, core geometry degradation and heat up, hydrogen generation by metal oxidation, corium stratification, focusing effect, vessel failure, induced failure by hot temperatures and pressures, High Pressure Melt Ejection (HPME) and displacement, Direct Containment Heating (DCH), In-Vessel Melt Retention (IVMR), Molten Core Concrete Interaction (MCCI), steam explosion,

hydrogen explosion, Deflagration to Detonation Transition (DDT), iodine chemistry, pool scrubbing, fission products filtering and characterization of radioactive releases.

Among the mitigating systems performance available to simulate in MAAP, it is to be noted the possibility of modelling external sources of mass and energy directed in-vessel or ex-vessel, i.e. standing for portable equipment.

The MAAP code version used in the simulation is the 5.02.

3.3   MELCOR

MELCOR [3,12,13,22,38] is a fully integrated severe accident code able to simulate the thermal-hydraulic phenomena in steady and transient condition and the main severe accident phenomena characterizing the RPV, the RC, the containment, and the confinement buildings typical of LWR. The estimation of the source term is obtained by MELCOR code as well. MELCOR is being developed at Sandia National Laboratories for the US Nuclear Regulatory Commission (NRC). The code is based on the "control volume" approach. MELCOR can be used with the Symbolic Nuclear Analysis Package (SNAP) [39] to develop the nodalization and for the post processing of data by using its animation model capabilities.

MELCOR has a modular structure and is based on packages. Each package simulates a different part of the transient phenomenology. In particular the Control Volume Hydrodynamics (CVH) and Flow Paths (FL) packages simulate the mass and energy transfer between control volumes, the Heat Structure (HS) package simulates the thermal response of the heat structure, the Core (COR) package evaluates behavior of the fuel, core and lower plenum structures including the degradation phenomena, Cavity (CAV) package models the core-concrete interactions, and the Radionuclide (RN) package characterizes the aerosol behavior, transport, dynamics and deposition, and removal by engineering safety features. It is to underline the role of the CVH/FP packages that provides the boundary condition for other packages.

The validation of the MELCOR code is based mainly on comparison with analytical results, code to code benchmark with other validated computer codes, validation against experimental data, and comparison to published real accident/events.

4   NODALIZATION DESCRIPTION

4.1   ASTEC v2 Plant Model Description

The ASTEC models for the containment, primary system and secondary system are depicted in Figure 4-1, 4-2 and 4-3 respectively (as taken from the IRSN report; [33,34]). The core is divided into 6 radial and 16 axial segments, and main internals such as core barrel, baffle, plates and columns are considered. Figure 4-2 shows 2 out of the 3 loops (including the one having the PRZ). The containment is divided in 13 volumes, Figure 4-1, each of them representing the main zones such as RC, dome, SGs, sump, etc. Primary circuit models 3 independent loops (HL, PRZ, SG tubes and legs, intermediate leg, main pump and CL), and includes some parts of the vessel (UP, UH and collector). Secondary circuit includes the SGs and SL.

Safety systems such as ECCS, containment sprays, RPS, and EFWS, pumps, relief valves, etc. and their functioning logics are modelled as close as possible to a generic real plant.
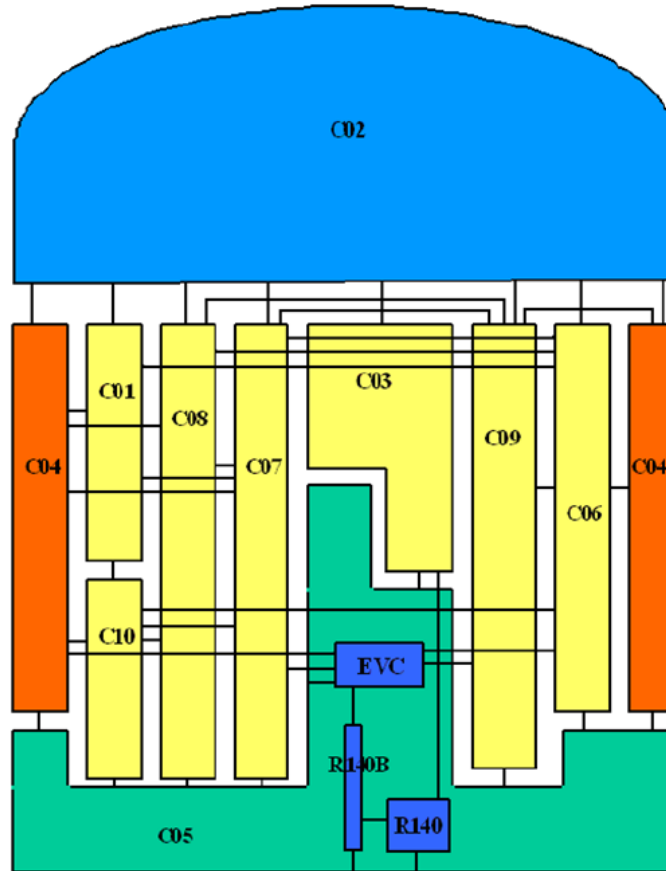
Figure 4-1 ASTEC Nodalization of the Containment of the Generic PWR 900 MWe Reference Reactor [33]

Figure 4-2 ASTEC Nodalization of the Primary Circuit of the Generic PWR 900 MWe Reference Reactor [33]

Figure 4-3 ASTEC Nodalization of the Secondary Circuit of the Generic PWR 900 MWe Reference Reactor [33]

4.2 MAAP 5.02 Plant Model Description

The MAAP 5.02 parameter file was developed accounting for the plant information data taken from the 2013 Foucher reports [33,34], and the ASTEC input files provided by IRSN during the EU-CESAM project. The MAAP5 3-loop RCS nodalization is depicted in Figure 4-4.

4.2.1 Core Model

The following in-plant information has been incorporated into the parameter file:
- The nominal and decay heat power;
- Type and number of fuel elements, mass and dimensions, and number of non-fuel rods;
- Masses and distribution of heat sinks (structural elements);
- 5 radial and 26 active axial nodes;
- 2 additional non-active nodes have been considered below and above the active core region to account for the fuel and non-fuel pins extension until achieving the core upper and lower support plates;
- Cladding, grid spacers, support plates, core barrel and baffle masses, dimensions, and elevations;
- Mass of initial fission product elements in the core (without specifying the fraction of each nuclide present in each element);

4.2.2 Primary System

- Generic layout of the plant, distinguishing between one so-called break loop and two unbroken loops;
- Water masses, detailed geometrical plant characteristics, cooling flow distribution (distinguishing between core flow and BP flow);
- Safety and relief valves of the PRZ, level and instrumentation level of the PRZ;
- Thermodynamic conditions;
- Heat sinks (structural elements) in terms of material, mass, and location.

4.2.3 Secondary System

- Geometrical characterization of the SGs;
- Connections with the EFWS, MFWS and main SLs;
- Water mass and elevation;
- Safety and relief valves of the secondary side;
- Thermodynamic conditions.

4.2.4 Containment

- Containment layout (see Figure 4-5): distribution of the different compartment in terms of volume versus height tables, geometry and connections:
  - C02 has been split into 3 and 10 to better track the containment dome;
  - C07-C09 are renamed as 6-8;
  - C01 is renamed as 9;
  - C06 has been assumed to host the entire reactor vessel and renamed as 2, including the lower compartment, namely the empty interfacing volumes with all

the rest of the volumes hosting the steam generators and pressurizer. The refueling cavity (C03) has been added up to this compartment;

- o C04, C05 and C10 have been assumed to build up the annular compartment;
- o R140 has been assumed as the RC, which together with R140 –having been assumed as the instrument channel in connection with the reactor cavity upwards to the seal table located in EVC (renamed 5), constitute compartment 1.
- o Compartment 1 and 5 (the latter only in case of HPME), are assumed to be able to contain corium debris pool;
- o All the atmospheric junctions have been implemented (as MAAP does not require additional information to allow liquid flow between compartments);

- Containment heat sinks: the 187 heat sinks indicated in the ASTEC report have been lumped into a total of 82 heat sinks attending to their material, geometrical dimensions and interfaces;

4.2.5 Safety Systems

- All the information found on the ASTEC input and output files regarding safety systems delays, pump curves, water mass inventories, etc., has been implemented accordingly: ECCS, containment sprays, RPS, and EFWS.
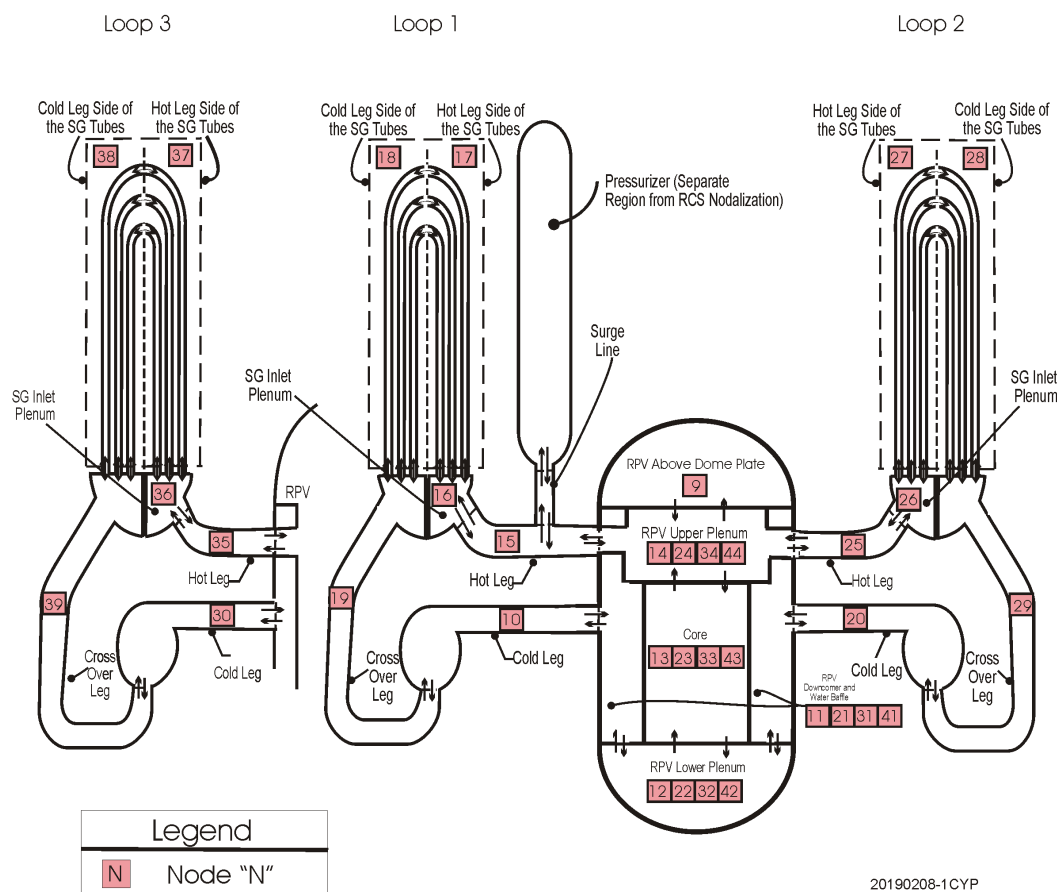
Figure 4-4   MAAP5 3-loop RCS Nodalization [40]
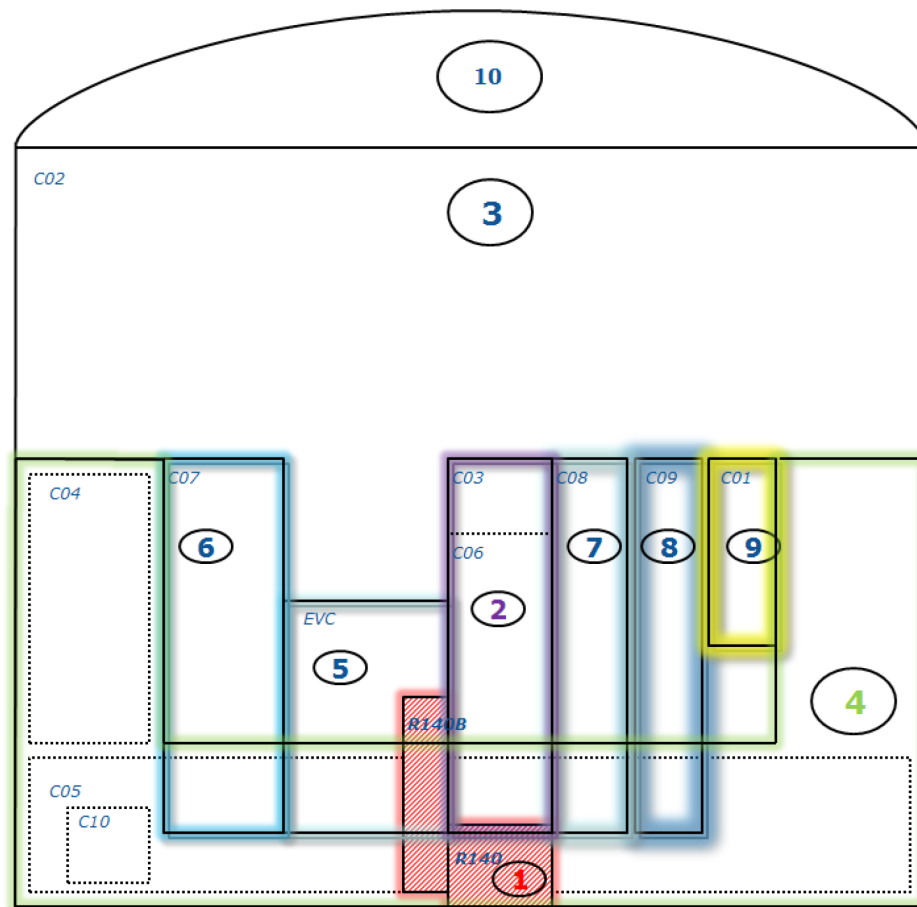
Figure 4-5 MAAP Nodalization of the Containment of the Generic PWR 900 MWe Reference Reactor

4.3 MELCOR Plant Model Description

MELCOR nodalization [28-30], developed by using SNAP [39], was designed to have a reasonable computational time and a realistic prediction of the thermal hydraulics and core degradation phenomena involved during a postulated transient assuring a reliable and accurate transient simulation. It has developed considering the plant information's reported in the 2013 Foucher reports [33,34], and the ASTEC input files provided by IRSN during the EU-CESAM project.

The three different loops are modelled separately; each loop consists of the HL, SG primary side (U tubes), the loop seal, the pump and the CL. It is to underline that the loop seal is modelled with only one CVH volume. All the U tubes are modelled with two equivalent hydraulic regions; one region represents the ascending U tubes side and the other represents the U tubes descending side; the SG inlet and outlet channel are modelled separately from the U-tubes CVH volumes. The PRZ and the related surge line are modelled separately as well; the PRZ is modelled with only one equivalent CVH volume thermally coupled with one heat structure representing the PRZ external shell. The surge line is modelled separately from the PRZ with

only one CVH volume. The three loops and RPV heat losses are modelled. The U tubes ascending side is coupled with the riser of the correspondent secondary side by a heat structure. The descending part of the U tubes is coupled with the riser of the correspondent secondary side by another heat structure. The SG secondary side is composed of three different volumes representing the SG downcomer, the SG riser and the SG cavity. The SRV and the PORV valves are modelled. The three PRZ SRV trains are modelled separately.

The thermal hydraulic CVH nodalization of the RPV is modelled with different hydraulic regions simulating the lower plenum, the core, the BP core, the UP, the UH and the DC. The UH flow and the BP flow are modelled. Figures 4-6 and 4-7 show, respectively, the overall RCS thermal hydraulic MELCOR nodalization and a detail of the primary side loop1 thermal hydraulic nodalization.

Figure 4-6 MELCOR Nodalization of the Generic PWR 900 MWe Reference Reactor, Developed by Using SNAP

Figure 4-7 MELCOR Loop 1 Nodalization of the Generic PWR 900 MWe Reference Reactor, Developed by Using SNAP

The core is modelled by a single hydraulic region, CVH package, coupled with the correspondent MELCOR code model of the COR package. The Core, in the COR package, Figure 4-8, is modelled with 17 axial regions and 6 radial regions; 5 radial regions are used to model the core region (in agreement with ASTEC and MAAP nodalization). The lower plenum is modelled with 7 axial regions and the core with the remaining 10 axial regions. All the supporting and non-supporting steel masses, Zircaloy masses, non-supporting Poison masses, and fuel Uranium masses are considered in the CORE Package nodalization. 82.3 tons of fuel and 19.23 tons of Zircaloy are considered in the COR package. Figure 4-8 shows the MELCOR nodalization of the core (COR package) developed by using SNAP. The lower head is composed of 13 rings with 10 lower head nodes. The candling heat transfer, the lower head failure modelling, the in-vessel falling debris quench model are activated. A hemisphere is used as a lower head type.

The containment in the MELCOR nodalization is modelled with one equivalent hydraulic volume coupled with several heat structures (18 equivalent heat structures) having the same heat transfer area and deposition surface and the same thermal inertia of the structures modelled in ASTEC input deck. A separate hydraulic volume modelling the cavity is considered.

The MELCOR modelling parameters used in the early SOARCA project [38] or the code default values [12] are used in the present work. The value of 2800 K is used for the melting temperature for Uranium-dioxide and Zirconium-oxide [38]. Currently, the code developers recommend a value of 2500 K for this parameter. However, to account for the uncertainties, the recent SOARCA Sequoyah study [41] used a normal distribution for this parameter with a mean of 2479 K and a standard deviation of 83 K.

The comparison of some of the main hydraulic volume characteristics of ASTEC, MAAP and MELCOR nodalization are reported in Table 4-1 while Table 4-2 shows SEBIM valves characteristics.

Figure 4-8 MELCOR 3D Core Nodalization Representation (COR package) of the Generic PWR 900 MWe Reference Reactor, Developed by Using SNAP

.

Table 4-1 Nodalization Volumes Comparison [33]

Volume (m3)	ASTEC		MAAP	MELCOR	
Primary Side Loop					
HL	2.75		2.75	2.75	
Water Box SG Hot Side	5.48			16.98	
SG Ascending Side	10.38				
TOP U Tube	2.24	33.23	33.23	-	33.23
SG Descending Side	10.38			16.25	
SG Water Box Cold Side	4.75				
Loop Seal	5.14		5.14	5.14	
CL	7.674		7.674	7.674	
Surge line	1.352		*	1.352	
PRZ	42.42		42.42	42.42	
Secondary Side					
SG Riser	75.75		-		
Cavity	75.68	151.43	-	151.43	
SG DC	24.47		-	24.47	
TOT SG	175.94		-	175.94	

MAAP: Surge Line D: 0.293m; L: 20.09 m.

Table 4-2 Primary Safety Valve Characteristics [reference ASTEC input-deck]

VALVE	P Set Points	NOTE
PRZ		
SEBIM 1	1.66 e7 Pa	MAAP: Dead band 6 bar Discharge coefficient 1
SEBIM 2	1.70 e7 Pa	MAAP: Dead band 6 bar Discharge coefficient 1
SEBIM 3	1.72 e7 Pa	MAAP: Dead band 6 bar Discharge coefficient 1

5   CODE CALCULATIONS

5.1   Steady State Analyses

One benchmark exercise performed by ENEA and JRC with different codes has been considered for this activity. Table 5-1 shows the correspondence between the codes used and the Organization involved; the main code version and processor/operative system characteristics are presented as well.

Table 5-1 Organizations Involved, Code Versions and Processor/Operative System Characteristics

CODE	ORGANIZATION	CODE VERSION	OPERATIVE SYSTEM	PROCESSOR
ASTEC	JRC	v2.1.0.3	Windows 64 bit	Intel Xeon CPU ES-2637 v3 @ 3.50 GHz, 32 GB RAM
MAAP	JRC	5.02	Windows, 64 bit	Intel Xeon CPU ES-2637 v3 @ 3.50 GHz, 32 GB RAM
MELCOR	ENEA	2.1_6342	Windows, 64 bit	Intel(R) Core ™ i7-3630 QM CPU @ 2.40 GHZ

A steady state analysis, at the same reactor operational point, has been performed to analyze the different code steady state conditions congruence before starting the comparison of the SBO transient calculated data. At the end of the steady state phase, i.e., Start of the Transient (SOT), the three codes are characterized by comparable and stable initial conditions. Table 5-2 shows the comparison of the main parameters characterizing the primary and secondary system after reaching a stable state, where relative discrepancies (DISCR) (%) of MAAP and MELCOR, considering ASTEC steady state calculation as a reference for the comparison, are also reported.

From the beginning of the transient analysis it is to underline that the three code Users have chosen different time plotting interval. ASTEC User chose a time plotting interval of 200s; this is larger in comparison with the time plotting interval used by MELCOR and MAAP Users in this application.

Table 5-2   Comparison of the Steady State Operational Conditions Predicted by ASTEC, MAAP and MELCOR Code

PARAMETERS	ASTEC	MAAP	MELCOR	MAAP DISCR (%)*	MELCOR DISCR (%)*
Primary side					
Pressurizer Pressure (bar)	155.16	155.89	154.78	0.47	0.24
Pressurizer Level (%)	50	49	50	2.00	0.00
Cold Leg 1 Flow Rate (kg/s)	4736	4738	4736	0.04	0.00
Core Flow Rate (kg/s)	13928	13894	13926	0.24	0.01
Upper Head Flow Rate (kg/s)	275	267	275	2.91	0.00
Primary Mass (kg)	185000	184535	185014	0.25	0.01
Inlet Core Temperature (K)	560	560	560	0.00	0.00
Outlet Core Temperature (K)	594.5	594.6	594.6	0.02	0.02
Secondary Side					
Separator Pressure (bar)	58	58	58	0.00	0.00
SG Water Mass (kg)	44385	44362	44385	0.00	0.00
SG Steam Mass (kg)	2725	-	2677	-	1.76
SG MFWS Flow Rate (kg/s)	512	-	512	-	0.00
Recirculation Ratio	4.15	4.15	4.15	0.00	0.00

MAAP and MELCOR discrepancy (%) is calculated against the operational point predicted by ASTEC code assumed as a reference.

5.2   Transient Analyses

5.2.1   Transient Thermal-Hydraulic Evolution: From the Initiating Event Until Core Heat-Up

After reaching stable and comparable steady state conditions, as described in the previous section, the SOT takes place. At the SOT, as hypothesized, the SCRAM and the consequent MSIVs/MFWs closure, and the Start of the pump coast-down are simulated by the codes. The SCRAM of the reactor (0s after the SOT) determines that the core power is in decay mode, Figure 5-1.

In this phase the three SGs remain the only heat sink of the residual power generated in the core (heat transfer in SG primary and secondary side). As underlined previously, after the SOT the isolation of the SG takes place; this determines a SG secondary side pressure increase in all the code calculation, due to the removal of the residual energy from the primary side. When the secondary side opening pressure set points are reached the SGs start releasing steam to the outside atmosphere. Cycling phase inception is predicted in all the codes considering the different valve logics implemented in the three code nodalization by the Code-Users. In ASTEC nodalization, the PORV valves located above the SGs are not physically modelled as "valves", but instead an adjustable opening cross-section is defined according to the function the valve must carry out (relief, cooling down, bleed, etc.). The performance of the secondary side safety valves in MAAP5 comprises the specification of so-called accumulation and blowdown opening

and closing dynamic performance which sets different opening area versus pressure moving relationships depending on whether the valve is already opened or closed. The reason why these valves do not cycle in MAAP for this case has strongly to do with such dynamic opening and closing setpoints. In MELCOR nodalization an opening and closing pressure valve set points are implemented determining an evident cycling of the secondary side pressure. It is to underline also that the time plotting interval of MELCOR calculation, selected by the code-user, is the finest in this part of the transient.

Figure 5-2, 5-3 and 5-4 show the comparison of the SG1, SG2 and SG3 pressure versus time predicted by ASTEC, MAAP and MELCOR code, respectively. Figure 5-5, 5-6 and 5-7 show the comparison of the SG1/2/3 pressure predicted by each code respectively. In this first phase of the transient the SG secondary pressure behavior predicted by each code is consistent for each loop from a qualitative and quantitative point of view.

The SG opening, and cycling determine a SG mass inventory decrease as underlined in the Figures 5-8, 5-9 and 5-10 representing, respectively, the comparison between the SG mass inventory predicted by ASTEC, MAAP and MELCOR in the three different loops. Figure 5-11, 5-12 and 5-13 show the SG1/2/3 mass inventory predicted by ASTEC, MAAP and MELCOR, respectively, in each loop. Figure 5-14 shows the comparison of the total primary to secondary heat transfer predicted by the three codes. From Figures 5-11, 5-12 and 5-13 it is possible to see that the SG mass inventory decrease is characterized by a symmetric behavior in all the SGs during the transient.

In the first phase of the SG cycling, the secondary side can remove the core residual power. Due to a negative balance between the decay heat and the heat transfer from the primary to the secondary side, the primary pressure decreases reaching a quasi-steady state phase as predicted by all the codes and depicted in Figure 5-15. Figure 5-16, 5-17 and 5-18 show the primary pressure behavior predicted by ASTEC, MAAP and MELCOR, respectively, and some of the main thermal hydraulics/core degradation relevant aspects. Table 5-3 summarizes the main relevant thermal hydraulic aspects related to this phenomenological window that we are going to analyze.

Table 5-3   SGs and Primary Cycling Events Predicted by ASTEC, MAAP and MELCOR Code

CODE	SG1,2,3 Cycling Inception (s)*	SG Heat Transfer Close to Zero or Inversion (s)	End of Primary P Quasi-SS Phase (s)	SEBIM Cycling Inception (s)	SEBIM Stuck Open (s)	DISCR (%) SEBIM Inception **	DISCR (%) SEBIM Stuck Open **
ASTEC	200	5150	1600	4200	9200	-	-
MAAP	100	5200	1300	3757	10099	10.55	9.77
MELCOR	30	3744	3100	4058	9414	3.38	2.33

*ASTEC plotting time interval, selected by the code user, is of 200s. Further ASTEC calculated data are available from 200s. Therefore, this value is not representative. Then the perceptual discrepancy of the codes is not calculated.
**ASTEC calculated data discrepancies based on the comparison with MAAP and MELCOR calculated data.

After the secondary side water depletion, the decay heat transfer almost drops to negligible values leading to the primary pressure increase as reflected in all three codes. ASTEC

calculations show a delayed and quite parallel to MAAP calculation primary pressure increase (Figure 5-15). MAAP shows an anticipated primary pressure increase in comparison with ASTEC. MELCOR shows the more delayed but rapid primary pressure increase; this determines a very close inception of the SEBIM valve in comparison with ASTEC. ASTEC discrepancies in comparison with MAAP and MELCOR code related to the primary side valve (SEBIM) intervention are at maximum of about 10%.

Single-phase natural circulation in the primary side and heat transfer in a covered core are the main thermal-hydraulic phenomena characterizing this early phase of the transient in the primary side. Figure 5-19 shows the comparison between the liquid mass flow rate in HL-Loop1 predicted by ASTEC, MAAP and MELCOR codes. Figure 5-20 and 5-21 show the comparison of the liquid mass flow rate in HL-Loop2 and 3, respectively, predicted by ASTEC, MAAP and MELCOR. It is worth mentioning that the three codes predict the same qualitative behavior though some quantitative discrepancies are observed. MAAP and MELCOR compute higher primary natural circulation mass flow rate compared with ASTEC. MELCOR shows a higher primary natural circulation flow rate in comparison with MAAP as well. This could be due to the different nodalization strategy used to model the loops between the codes. For instance ASTEC loop nodalization is characterized by five volumes for modelling the HL and CL, three volumes for modelling the loop seal and 15 volumes for modelling the SG primary side; MELCOR nodalization is characterized by one volume for modelling the HL, CL and loop seal, and four volumes for modelling the SG primary side, whereas MAAP uses a fixed nodalization modelling the HL, CL, and intermediate leg with 1 single node, respectively. Figures 5-22, 5-23 and 5-24 represent the mass flow rate predicted by ASTEC, MAAP and MELCOR for the HL 1, 2 and 3 respectively; they show that in this phase of the transient the mass flow rate loop behavior is symmetric in all the loops for each code prediction.

The cycling phase of the secondary side determines a secondary side water inventory decrease causing a decrease of the secondary side heat removal capability as shown in Figures 5-8 to 5-14. It is to underline that MELCOR code shows a small quantity of water inside the SG for a longer time in comparison with MAAP and ASTEC code. This is an immediate consequence of the well-known definition of "pool fraction" in MELCOR code. The pool fraction in MELCOR code represents the fraction of the heat structure thermally coupled with the pool of the connected CVH volume. In general, in MELCOR, for each heat structure it is possible to define a "critical pool fraction for pool (CPFPL/R)" and critical "pool fraction for atmosphere (CPFAL/R)". The CPFPL/R represents the minimum value of the pool fraction for considering the heat transfer to the pool at the selected surface of the heat structure –left (L) or right (R) (0< CFPL/R<1). The CPFAL/R represents the maximum value of the pool fraction for considering the heat transfer to the atmosphere at the selected surface of the heat structure (0< CPFAL/R<1). To avoid numerical problem due to heat transfer with arbitrarily small fluid mass the User has used for this analysis CPFPL/R = 0.02 and CPFAL/R = 0.98. These parameters are imposed by using the sensitivity coefficient 4071 (Bounds on Critical Pool Fraction) in the MELCOR nodalization. This is a useful and flexible parameter for the Code-User.

Figure 5-14 shows the comparison of the total power transferred from the primary to the secondary side predicted by ASTEC, MAAP and MELCOR code. In relation to the MELCOR data it is to underline, as expected, that the small quantity of liquid water remaining in the SGs do not practically contribute to the primary to secondary side heat transfer. In fact, when the pool fraction of the ascending/descending side SG heat structure, coupled with secondary side volume -Right-, is less than the User value of 0.02, the heat transfer takes place only between the heat structure and the atmosphere; this determines a sensible reduction of the SG primary

to secondary heat transfer. Only two small peaks of the heat transfer, determining a small and temporary pressure peaks in the secondary side, are observed (in these instants the CPFPR is temporary greater than 0.02).

During this first phenomenological window the three codes predict the same qualitative behavior though some quantitative minor discrepancies are present. It is to underline that a different primary pressure minimum value is predicted by MAAP code in comparison with MELCOR and ASTEC code, Figure 5-15; this, coupled with the anticipated (in comparison with ASTEC and MELCOR) end of the quasi-steady state phase of the primary system, determines a different inception of the primary SEBIM valves cycling phase in the MAAP calculation.

The cycling phase of the secondary side determines a secondary side water inventory decrease causing a decrease of the secondary side heat removal capability. Figure 5-14 shows that, in relation to the primary to secondary heat transfer, all the codes predict the same qualitative and quantitative (with some difference) behavior in this transient phase. The sensible decrease after the SCRAM and the progressive decrease of the primary to secondary heat transfer, during the single-phase natural circulation, are predicted by all the codes. It is to underline that while MAAP starts to assume a primary to secondary heat transfer of about 0 W at about 5200s after the SOT (with SG1, 2 and 3 liquid mass of about 28 kg each) ASTEC code at about 5150s starts to assume some negative values (at about 5150-5250s; about 8150-8500s; about 8900-9100s; about 9300-10200s; about 10300-11000s) determining a heat transfer between the secondary to the primary side (at about 5200s the SG1, 2 and 3 liquid mass is about 0 kg). MELCOR code at about 3744s after the SOT starts to show a small positive value due to the heat transfer between the UT ascending/descending heat structure and the SG riser atmosphere. In this situation the pool fraction of the ascending/descending side SGs heat structure coupled with the secondary side volume (Right) is less than the User value of 0.02. A few heat transfer spikes are predicted by the code due to a temporary increase of more than 0.02 of the pool fraction, Figure 5-14 (in particular the SG1 heat structure overpasses the 0.02 at about 4324s after the SOT, the SG2 at about 4646s and SG3 at about 4648s; these instants correspond to a primary to secondary heat transfer spikes and the consequent secondary pressure spikes at 4326s in the loop1, 4648s in the loop2, and 4650s in the loop3). A temporary small negative heat transfer is predicted by MELCOR code (9493-10439s). It is interesting to underline that both ASTEC and MELCOR predicts this negative primary to secondary heat transfer.

Before arriving at the SGs secondary side dry-out, the decrease of the SGs secondary side inventory determines the decrease of the SGs removing capability. Then all the codes predict the end of the primary side quasi steady-state phase and the beginning of a primary pressure increase (primary system pressurization). In particular, Table 5-4, in ASTEC calculations the primary pressure increase starts at about 1600s after the SOT while MSG1=16900 kg (~40%), MSG2=17500 kg (~40%), MSG3=17400 kg (~40%) as shown in Figure 5-11 and 5-16; in MAAP calculations the primary pressure increase starts at about 1200s after the SOT while the MSG1= 22121kg (~50%), MSG2=22635 (~50 %), MSG3=22635 (~50 %) as shown in Figure 5-12 and 5-17, in MELCOR calculations the primary pressure increase starts at about 3100s after the SOT while the MSG1=5204 kg (~12%), MSG2=5943 kg (~14%), MSG3=5941 kg (~14%) as shown in Figures 5-13 and 5-18. It is to underline that while in ASTEC and MAAP code the primary pressure increase starts when the secondary side mass inventory is between the 40 and 50%, in MELCOR code it starts when the secondary mass inventory is at about 10-15%. However as previously underlined the discrepancy of ASTEC calculated data in comparison with MAAP and MELCOR calculations, regarding the SEBIM valve inception, is at maximum of about the 12%. Table 5-4 shows the SG secondary side mass inventory, in the three codes, at the end of the primary side quasi-steady state.

Table 5-4 SGs Secondary Side Mass Inventory at the End of the Primary Side Quasi-Steady State

Time	ASTEC			MAAP			MELCOR		
	SG1	SG2	SG3	SG1	SG2	SG3	SG1	SG2	SG3
MSG (t=0) [kg]	44385	44385	44385	44362	44330	44330	44385	44385	44385
MSG (end of primary SS) [kg]	16900	17500	17400	22121	22635	22635	5204	5943	5941
Liquid Mass Reduction [%]	38.08	39.43	39.20	49.86	51.06	51.06	11.72	13.39	13.39

When the primary pressure set points are reached, the SEBIM cycling phase starts. As underlined in the Figures 5-15 to 5-18, all the codes predict the cycling phase of the SEBIM valves, with different cycling phase determined by the different User approach used to model the logic of valve and the valves parameters. During the first part of the SEBIM cycling phase the primary system is still in single phase natural circulation. The time plotting interval has a role in the primary pressure cycling representation as well.

Single-phase natural circulation predicted by the codes as shown in Figures 5-19 to 5-21 continues till void formation starts (two-phase natural circulation) in the primary side. Considering as a reference the fluid condition in the HL, Table 5-5, the two-phase flow starts in ASTEC at about 6400s after the SOT in the loop1, in MAAP at about 6404s after the SOT in the loop1, and in MELCOR at about 6300s after the SOT in the loop 1. When the two-phase natural circulation starts a decrease in the mass flow rate is predicted by all the codes. Figures 5-22, 5-23 and 5-24 show ASTEC, MAAP and MELCOR mass flow rate in all the three loops respectively for each code. It is to underline that in this phase, each code predicts the same qualitative mass flow rate behavior in all the three loops. In all the codes the void inception in the HL is contemporaneous for all the loops, Table 5-5. ASTEC discrepancies in comparison with MAAP and MELCOR code related to the two-phase flow inception in HL are less than 2%. Core thermal hydraulic behavior is still characterized by heat transfer in covered core.

Table 5-5 Two Phase Flow Inception in the HLs Predicted by ASTEC, MAAP and MELCOR

CODE	Loop1 (s)	Loop2 (s)	Loop3 (s)	DISCR* (%) L1	DISCR* (%) L2	DISCR *(%) L3
ASTEC	6400	6400	6400	-	-	-
MAAP	6404	6404	6404	0.06	0.06	0.06
MELCOR	6300	6300	6300	1.56	1.56	1.56

* ASTEC calculated data discrepancies based on the comparison with MAAP and MELCOR calculated data.

In relation to the secondary side behavior, ASTEC shows the same qualitative behavior in the three SGs but with a quantitative difference between the SG1, where the PRZ is connected, with respect to the SG2 and 3, Figure 5-5. The SG1 pressure is higher than the SG 2 and 3 starting from about 6600s after the SOT; in this time the SG is already empty of liquid. MAAP shows the same qualitative and quantitative pressure behavior in the three different SGs (Figure 5-6). MELCOR code shows the same qualitative and quantitative behavior in the three SGs but with some small quantitative difference in the valve cycling phase (Figure 5-7).

5.2.2 Transient Core Degradation Evolution: Core Heat-Up Phase, Oxidation Process and Core Relocation

The water boil-off of the primary fluid causes a steady evaporation of the primary coolant fluid with a consequent fluid level decrease in the core; this determines, as underlined in the Table 5-6, that a core uncovering process (TAF is uncovered) starts in the three codes at about 8000s for ASTEC, 8083s for MAAP and at about 7000s for MELCOR. The consequent steam formation determines a decrease of the primary fluid cooling capability with a consequent decrease of the energy removed from fuel rods. A consequent increase of the cladding temperature takes place. The thermal hydraulic behavior of the core starts to be characterized by heat transfer in uncovered core. Since the energy removed from the primary coolant is less than the decay heat generated in the core a fuel rod claddings heat-up phase starts as shown by Figure 5-25, 5-26 and 5-27. The steam formation determines the chemical reaction between the core material and the steam. The oxidation of Zircaloy is exothermic, therefore the energy released is coupled with the core decay power; this causes an acceleration of the core heat-up rate with a consequent temperature escalation; it starts the hydrogen generation as well. The oxidation of the steel structure takes place as well, but it is less significant than Zircaloy oxidation because the steel oxidation is less energetic and the area interacting with steam is less than Zircaloy area. It is to underline that in a generic PWR-900 the control rod poison is made of Ag-In-Cd that does not oxidize. The hydrogen generation starts at about 8400s for ASTEC code, 8795s for MAAP code, 8382s for the MELCOR code, as shown in Table 5-7. Figure 5-25, 5-26, 5-27 show the maximum intact cladding temperature predicted by each code along the different rings (for each ring it represents the maximum along the different axial cells). Figure 5-28 to 5-32 show respectively the comparison between the maximum intact cladding temperature predicted by ASTEC, MAAP and MELCOR. SEBIM valves stuck open at about 9200s for ASTEC, 10099s for MAAP and 9414s for MELCOR. It is to underline that while for MAAP and MELCOR it represents the "instantaneous" maximum intact cladding temperature, for ASTEC it represents the "absolute" maximum intact cladding temperature that has been reached from time zero.

Table 5-6 Core Uncovering Events Predicted by ASTEC, MAAP and MELCOR

CODE	Core TAF Unc (s)	Core BAF Unc (s)	DISCR (%) TAF Unc *	DISCR (%) BAF Unc *
ASTEC	8000	9400	-	-
MAAP	8083	10165	1.04	8.14
MELCOR	7000	9570	12.50	1.81

ASTEC calculated data discrepancies based on the comparison with MAAP and MELCOR calculated data.

Figure 5-25 shows the maximum intact cladding temperature predicted by the ASTEC code for the different 5 rings used to radially model the core. In this first phase of the core degradation, ASTEC predicts the same qualitatively intact clad temperature behavior for all the rings. From a quantitative point of view, rings 2 and 3 show a more rapid maximum temperature escalation than rings 1, 4 and 5.

Since in ASTEC it represents the "absolute" maximum intact cladding temperature that has been reached from the time zero, this parameter can never decrease but only increase or stay stable. This explains the difference between MELCOR and MAAP predictions.

Figure 5-26 shows the maximum intact cladding temperature predicted by the MAAP code for the different 5 rings. Rings 1,2,3,4 show a similar temperature escalation while ring 5 shows a certain delay. A first clad temperature peak (rings 1,2,3,4), more pronounced in the rings 2 and 3, is followed by a cladding temperature decrease following by a further cladding temperature increase. The intact cladding temperature decrease could be due to a formation of a two-phase flow in the core due to the SEBIM valve stuck opening. The same phenomenon is observed in the MELCOR code.

Table 5-7 Hydrogen Generation Characterization for the Three Different Code Calculations

CODE	H2 Start (s)	TCL 1300K (s) *	Heat up rate after T>1300 K (s)**	TCL 1855K (s) *	In-Vessel H2 Max (s)	DISCR (%) diff H2 start ***	DISCR (%) TCL 1300K ***	DISCR (%) TCL 1855K ***	DISCR (%) H2 max ***
ASTEC	8400	9970	> 1 K/s	10080	17000	-	.	-	-
MAAP	8795	10845	> 1 K/s	10904	20876	4.7	8.8	8.2	22.8
MELCOR	8382	8700	> 1 K/s	9248	19250	0.2	12.7	8.3	13.2

*For ASTEC code is analyzed the second ring behavior because it is the faster to increase the cladding T; for MAAP code is analyzed the second ring behavior in the upper part of the core (axial = 58/radial =1), because it is the faster to increase the cladding T; for MELCOR code is analyzed the first ring behavior at the 8th core level because it is the faster to increase the cladding T (the core is modelled by using 10 axial level).

** The heat up rate is an important parameter because permit the operator actions and influences the phenomenology of oxidation and liquid formation in the core.

***ASTEC calculated data discrepancies based on the comparison with MAAP and MELCOR calculated data.

Figure 5-27 shows the maximum intact cladding temperature for the different 5 rings predicted by MELCOR code. MELCOR code predicts the same qualitatively maximum intact clad temperature behavior for all the rings but with a different quantitatively time evolution. The same temperature decrease, related to the two-phase flow formation in the core due to the SEBIM stuck valve opening, is observed in the MELCOR code results, in agreement with MAAP code. MELCOR calculation is characterized by a greater cladding temperature decrease that determines a sensible reduction of the hydrogen generation rate causing a sensible change in the hydrogen mass production slope, Figure 5-33. This will increase again with the subsequent cladding temperature increase.

In relation to the primary side mass flow rate in this phase of the transient, Figure 5-22 to 5-24, MELCOR and MAAP code predict asymmetric loops behavior. In fact, in MELCOR calculation hot steam flow takes place in the loop 1 in the normal loop flow direction while in the loop 2 and 3 in the reverse flow direction. In MAAP calculation the same phenomenon takes place, but the mass flow rate is in the normal flow direction in the loop 2 while the loop 1 and 3 is in the reverse flow direction. In ASTEC calculation this phenomenon seems not taking place.

This phase of core degradation does not result in a loss of rod-like geometry; therefore, the general shape of the coolant flow path does not change (geometry effects).

The materials with a lower melting temperature than fuel (i.e., control rods, guide tubes, and grids) determine the starting of the melting and relocation phase of the core damage. Along the core degradation and melt progression phase, the cladding and fuel failure mechanisms and the consequent core materials transport/relocation take place. These phenomena determine a loss of core geometry with a consequent change of the coolant flow path shape. The hydrogen mass production is therefore dependent on the core degradation progression and the consequent

available area for the oxidation and flow blockage phenomena. Though there is uncertainty to correctly estimate the amount of area available and the effect of flow blockage, in general a significant amount of hydrogen could be produced during this phase of the transient and it is estimated by the codes considering their different core material degradation/relocation modelling capability. Considering these complex phenomena that take place in the core during this degradation phase, in order to visualize relevant degradation aspects as the time of failure of the different fuel rings, the core plate failure or shroud failure, the slumping progression, the vessel lower head failure, Table 5-8 summarizes the timing when the different rings fail in the three different code calculations, and Table 5-9 summarizes the core plate and vessel failure times.

Table 5-8 Upper Core Rings Failure Timing Predicted by ASTEC, MAAP and MELCOR

CODE	Upper Core Ring failure (s)				
	1	2	3	4	5
ASTEC*	10953	10953	11353	11753	12353
MAAP	12786	12724	12866	13484	14815
MELCOR**	11600	13100	13380	13650	14380

Considering Figure 5-38, where ASTEC core degradation/relocation visualization is reported, instead to consider the upper core ring failure, it is estimated the instant when the fuel ring continuity is lost.
** Upper part of the 5th ring starts to collapse at 14380s, but other axial levels continue their failure starting from 15270s. Some indications are shown in Figure 5-41.*

Table 5-9 Core Plate Failure Timing and Vessel Failure

CODE	Core Plate Ring failure (s)					Slumping Inception (s)	Vessel Failure (s)	DISCR (%) Slump. Inc.**	DISCR (%) Vessel Failure**
	1	2	3	4	5				
ASTEC	-*					16600	18157	-	-
MAAP	15526					15526	20608	6.47	13.50
MELCOR	14585	14730	16035	16035	17485	14580	19250	12.17	6.02

No core plate failure has been predicted by ASTEC code but a lateral slumping through the shroud failure.
** ASTEC calculated data discrepancies based on the comparison with MAAP and MELCOR calculated data.*

Though a detail characterization and analyses of the core material relocation/distribution and the codes representation is out of the scope of the research activity presented here, the macroscopic effect of the hydrogen generation is analyzed here. ASTEC shows a general smooth progressive hydrogen production along the core degradation phase. MAAP code shows a general smooth progressive hydrogen production. MELCOR code shows instead a general progressive hydrogen production, but the previously mentioned stuck open SEBIM valve determines a sensible reduction and a subsequent increase (when the cladding temperature increases again) of the oxidation rate. This, coupled with the progressive upper ring core failure and the progressive relocation of the core in the lower plenum, determines the hydrogen production versus time behavior.

5.2.3 Transient Core Degradation Evolution: Core Relocation in the Lower Plenum and Vessel Failure

After the core material relocation into the lower plenum (slumping) additional hydrogen could be generated due to the oxidation phenomena. After the slumping, all the liquid water present in the lower plenum evaporates due to the relocation of the degraded core material which causes the increase of the RCS pressure in the short term. This part of the transient is strongly influenced by the core relocation scenario. In this application, while in MELCOR and MAAP, the slumping takes place through the core plate failure, in ASTEC, it takes place through the failure of the shroud as shown in Figure 5-38. The reasons for the difference between ASTEC and MAAP/MELCOR slumping behavior are not investigated since this issue was already discussed in [25].

By looking at the ASTEC calculated data, Figure 5-16, it is possible to see that the primary pressure peak related to the slumping phenomena is small in absolute value and short in time extension. The hydrogen production is characterized by a very small increase that permits to conclude that all the hydrogen is created before the slumping, Figure 5-34. The peak pressure predicted by MAAP (Figure 5-17) is characterized by a sensible absolute extension and by a small-time extension. The mass Hydrogen production is characterized by an increase of about 40 kg during the slumping phase, Figure 5-35. In relation to MELCOR code it is possible to see that the material located in the different rings relocate in the lower plenum in different instants, Table 5-9, determining a progressive production of steam with a consequent progressive pressure and hydrogen mass production increase, Figure 5-18 and 5-36. This determines a smaller in absolute value but a more extended primary pressure peak in comparison with MAAP and ASTEC. The Hydrogen mass production is characterized by an increase of about 70 kg during the slumping phase. In relation to the hydrogen production by the code it is important to note that ASTEC, MAAP and MELCOR produce a sensible different quantity of Hydrogen (Table 5-10). In general, hydrogen mass production is dependent also on how the slumping in the lower plenum takes place.

Table 5-10 Hydrogen Production Predicted by ASTEC, MAAP and MELCOR

CODE	H2 Before Slumping (kg)	Tot In Vessel H2 (kg)	DISCR (%) Before Slump*	DISCR (%) H2 TOT *
ASTEC	273	275	-	-
MAAP	151	191	44.69	30.55
MELCOR	309	377	13.18	37.09

ASTEC calculated data discrepancies based on the comparison with MAAP and MELCOR calculated data.

As underlined before, the hydrogen mass production is dependent from the core degradation progression and the consequent available area for the oxidation and flow blockage phenomena. Therefore, the discrepancies related to these parameters underline the modelling difference of the code related to core material degradation/relocation determining differences in the available area for the oxidation process, different flow blockage condition, and differences in the code node porosity predicted, etc. It is important to underline that the area available for the oxidation has a great uncertainty due to the complex phenomena taking place during the degradation and relocation of the core material and limited full-scale experiments.

By looking at the hydrogen generation mass behavior, Figures 5-34 to 5-36, and at the behavior of the intact cladding temperature, hydrogen generation increases when the intact cladding temperature reaches about 1300K; a further significant increase takes place when it reaches about 1855K. This determines an acceleration of the core heat up more than 1K/s in the code calculation, as underlined in Table 5-7. ASTEC discrepancies, in comparison with MAAP and MELCOR calculated data, of the time sequence related to the hydrogen generation are at maximum of about the 20%. The hydrogen mass behavior of MELCOR code is dependent from the progressive radial degradation of the core and the progressive failure of the core support plate. The hydrogen mass production, Figure 5-33 and the oxidation energy released, Figure 5-37, are consistent between the three codes (if the hydrogen produced is higher in a code also the oxidation energy is higher). The long-term phenomenological behavior is dominated by physical and chemical phenomena and boundary condition of the lower plenum. This determines the timing of the lower head failure, as shown in Table 5-9.

Table 5-11 summarizes the relevant phenomenological aspect time sequence of events predicted by ASTEC, MAAP and MELCOR. Figure 5-38 for ASTEC, 5-39/5-40 for MAAP and 5-41 for MELCOR (by using SNAP) show the representation of the core degradation/relocation evolution and morphologies predicted by the codes. A detail characterization of the code modelling differences is here not investigated but it is planned as a future activity.

Table 5-11 Summary of the Relevant Phenomenological Aspect Sequence of Events Predicted by ASTEC, MAAP and MELCOR

RELEVANT PHENOMENOLOGYCAL ASPECTS	ASTEC	MAAP	MELCOR	MAAP DISCR* (%)	MELCOR DISCR* (%)
SG1,2,3 Cycling Inception (s)	200	100	30	-	-
SEBIM Cycling Inception (s)	4200	3757	4058	10.55	3.38
Two Phase inception in the HL (s)	6400	6404	6300	0.06	1.56
Core TAF Uncovered (s)	8000	8083	7000	1.04	12.50
H2 Start (s)	8400	8795	8382	4.70	0.21
SEBIM Stuck Open (s)	9200	10099	9414	9.77	2.33
Core BAF Uncovery (s)	9400	10165	9570	8.14	1.81
TCL 1300K (s)	9970	10845	8700	8.78	12.74
TCL 1855K (s)	10080	10904	9248	8.17	8.25
Upper Core Ring Failure 1 (s)**	10953	12786	11600	16.74	5.91
Upper Core Ring Failure 2 (s)**	10953	12724	13100	16.17	19.60
Upper Core Ring Failure 3 (s)**	11353	12866	13380	13.33	17.85
Upper Core Ring Failure 4 (s)**	11753	13484	13650	14.73	16.14
Upper Core Ring Failure 5 (s)**/***	12353	14815	14380	19.93	16.41
Slumping Inception (s)	16600	15526	14580	6.47	12.17
Vessel Failure (s)	18157	20608	19250	13.50	6.02

*ASTEC calculated data discrepancies based on the comparison with MAAP and MELCOR calculated data.
**For ASTEC it is estimate the instant when the fuel ring continuity is lost.
** For MELCOR calculation, the upper part of the 5th ring starts to collapse at 14380s, but other axial levels continue their failure starting from 15270s. Some indications are shown in Figure 5-41.
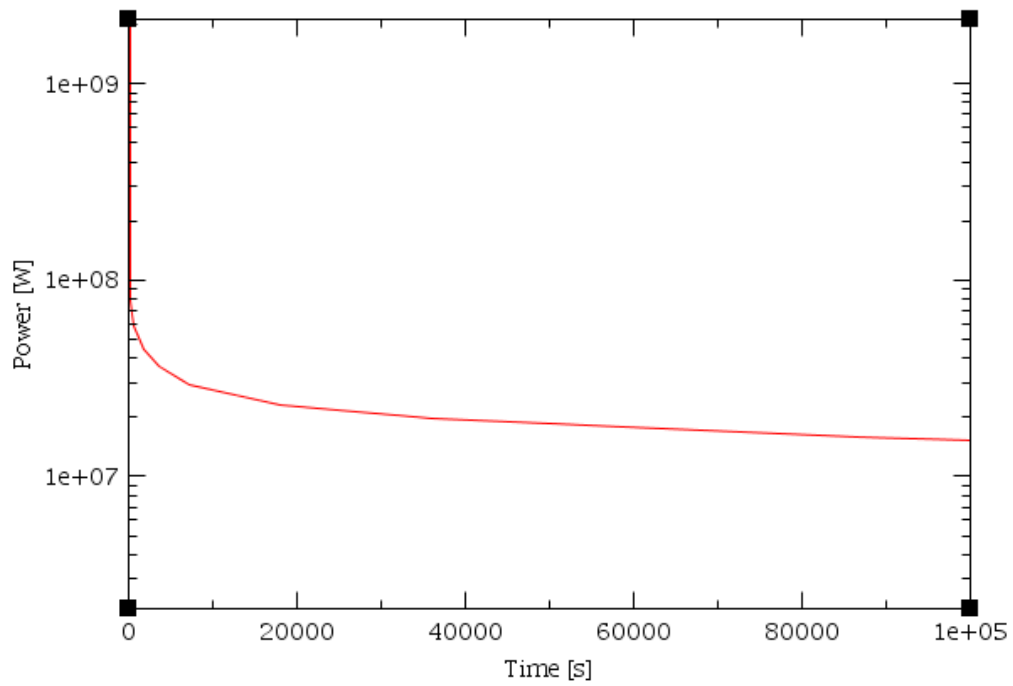
Figure 5-1 Decay Heat Versus Time Imposed in ASTEC, MAAP and MELCOR Nodalization
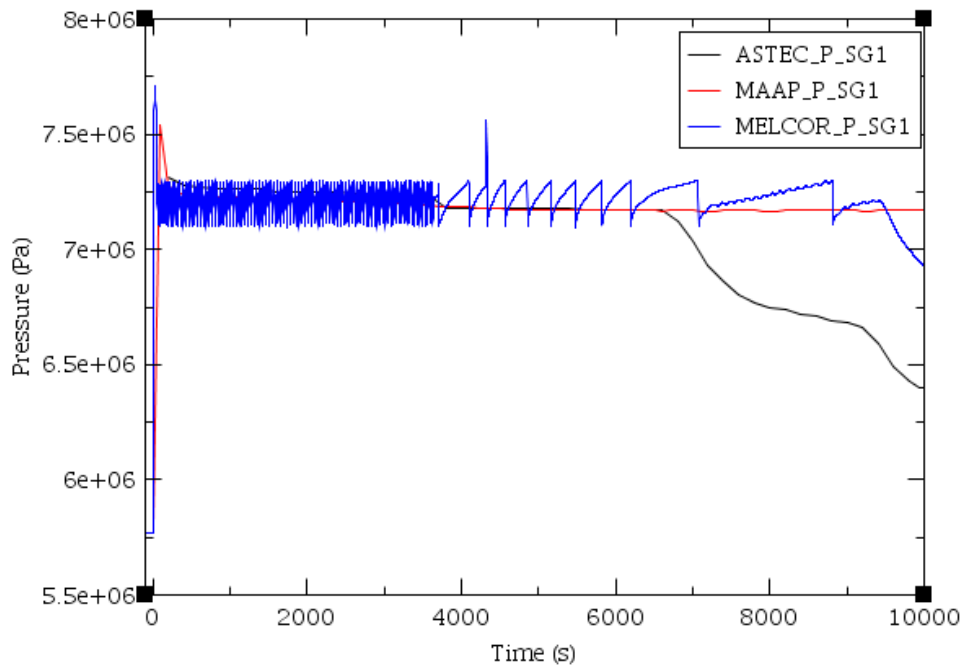

Figure 5-2 Secondary SG1 Pressure Versus Time Predicted by ASTEC, MAAP and MELCOR
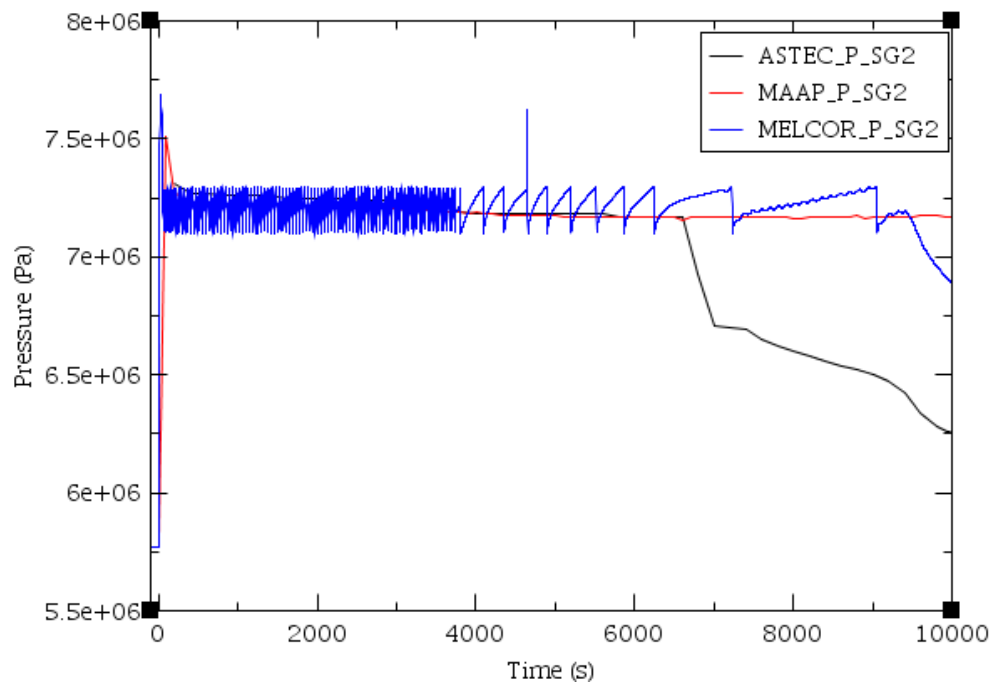
Figure 5-3 Secondary SG2 Pressure Versus Time Predicted by ASTEC, MAAP and MELCOR
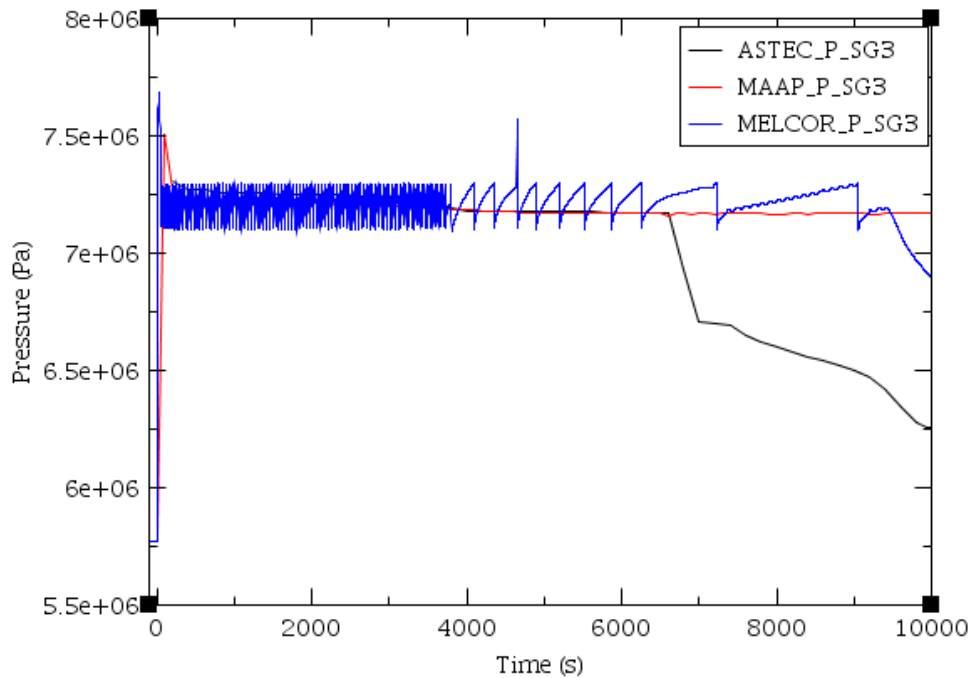

Figure 5-4 Secondary SG3 Pressure Versus Time Predicted by ASTEC, MAAP and MELCOR
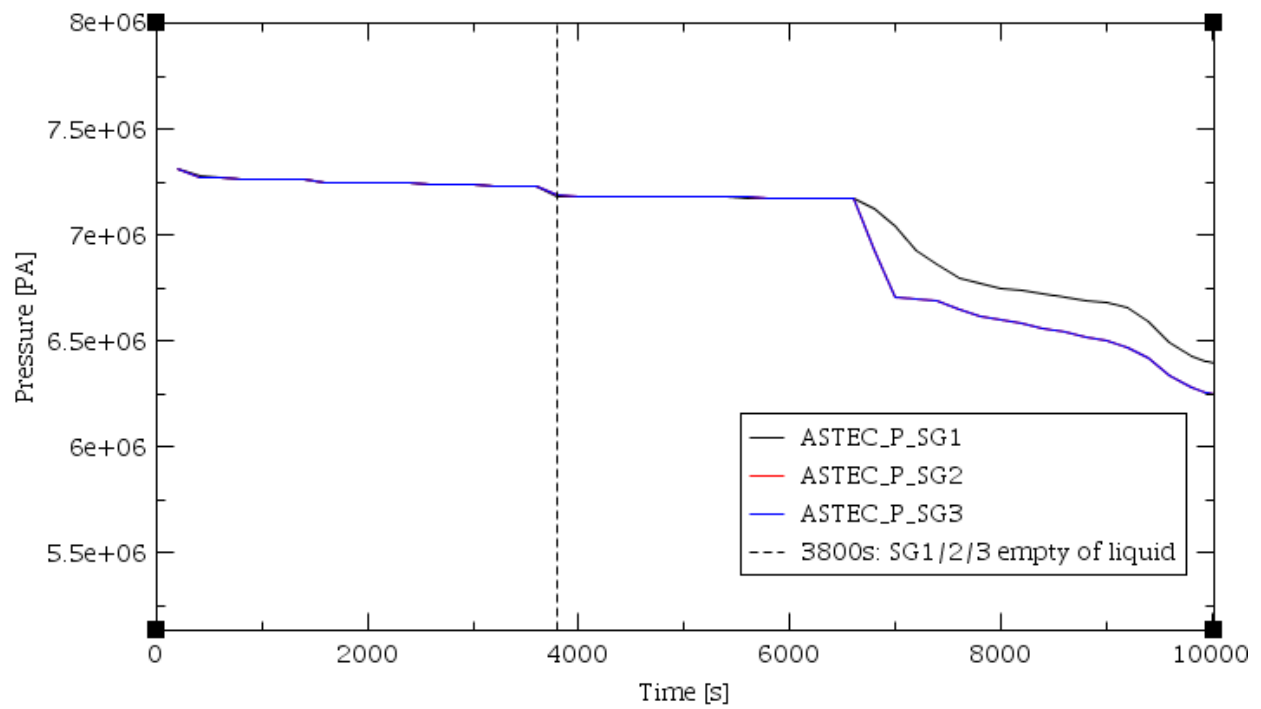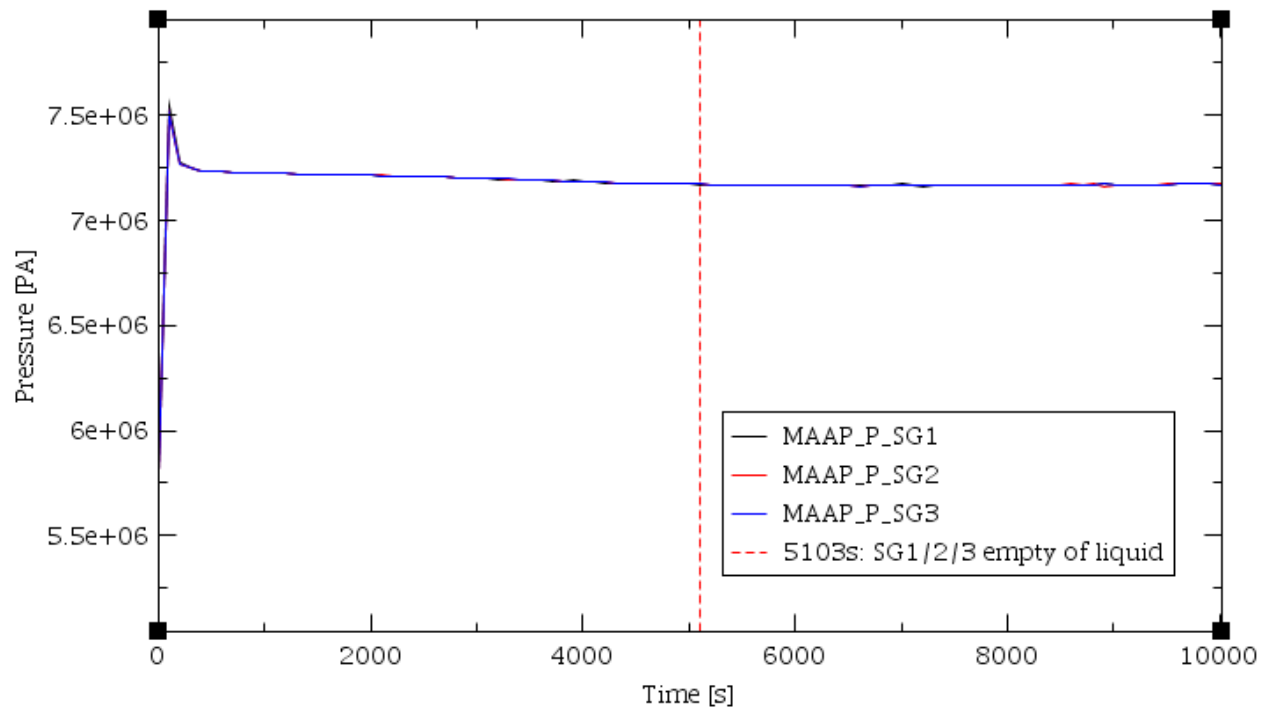
29

Figure 5-5 Secondary SG1/2/3 Pressure Versus Time Predicted by ASTEC

Figure 5-6 Secondary SG1/2/3 Pressure Versus Time Predicted by MAAP
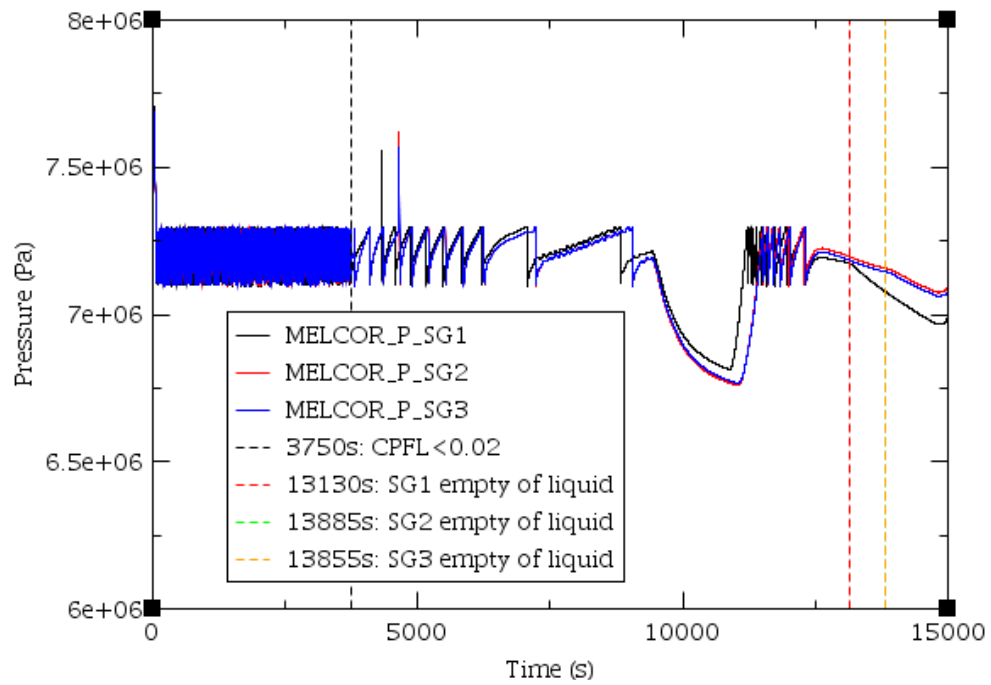
Figure 5-7 Secondary SG1/2/3 Pressure Versus Time Predicted by MELCOR
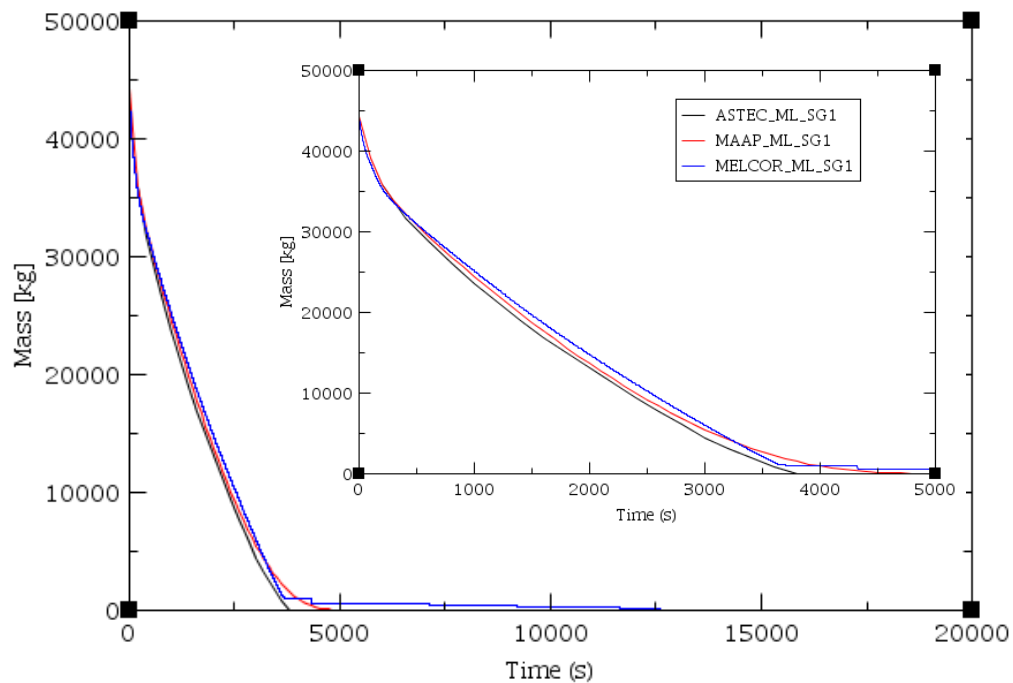
Figure 5-8 SG1 Liquid Mass Inventory Versus Time Predicted by ASTEC, MAAP and MELCOR
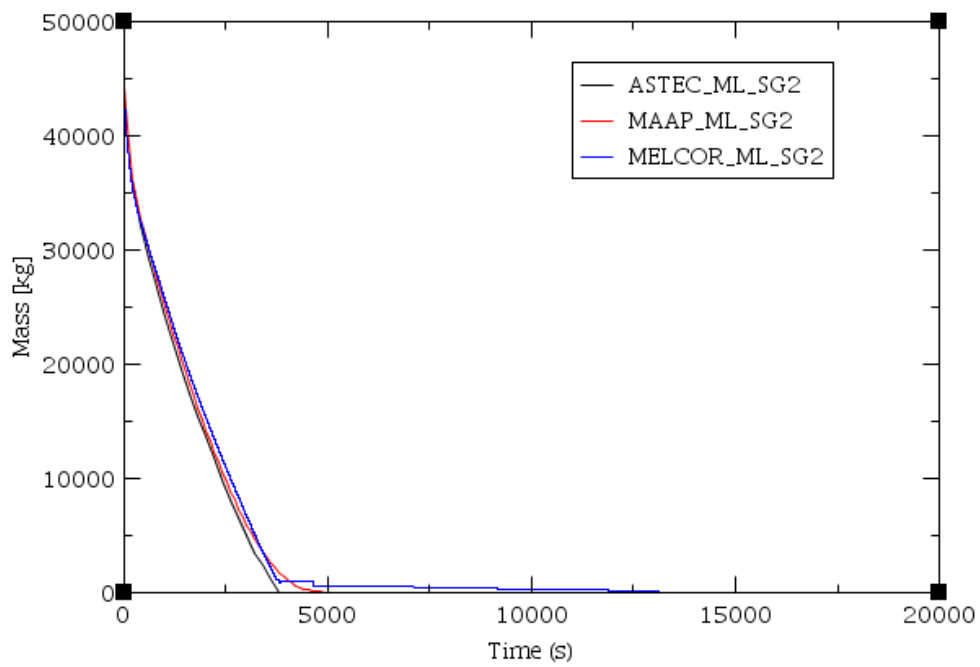
Figure 5-9 SG2 Liquid Mass Inventory Versus Time Predicted by ASTEC, MAAP and MELCOR
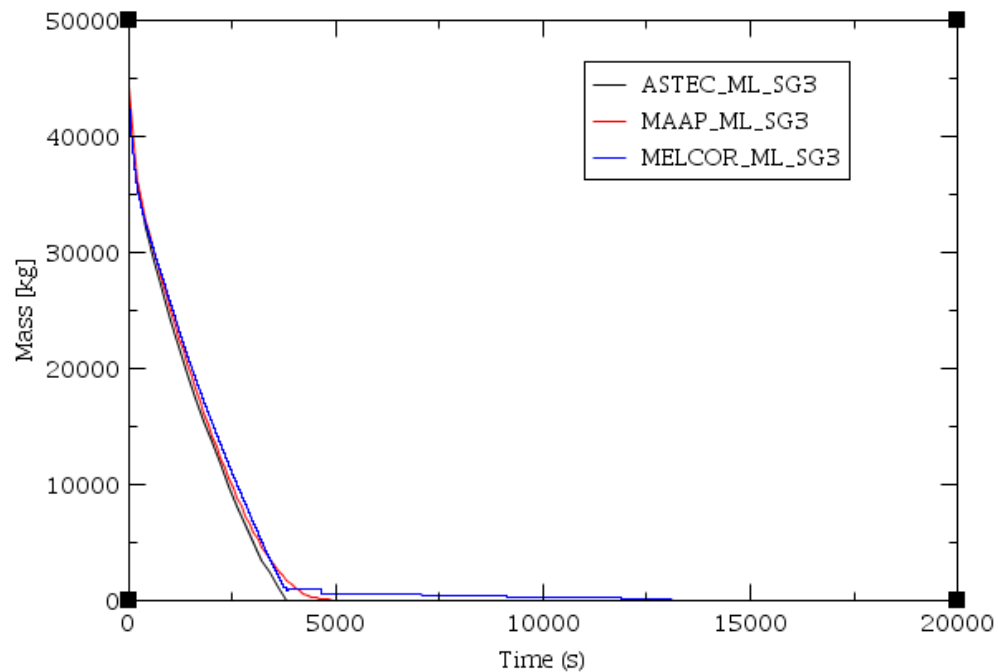
Figure 5-10 SG3 Liquid Mass Inventory Versus Time Predicted by ASTEC, MAAP and MELCOR
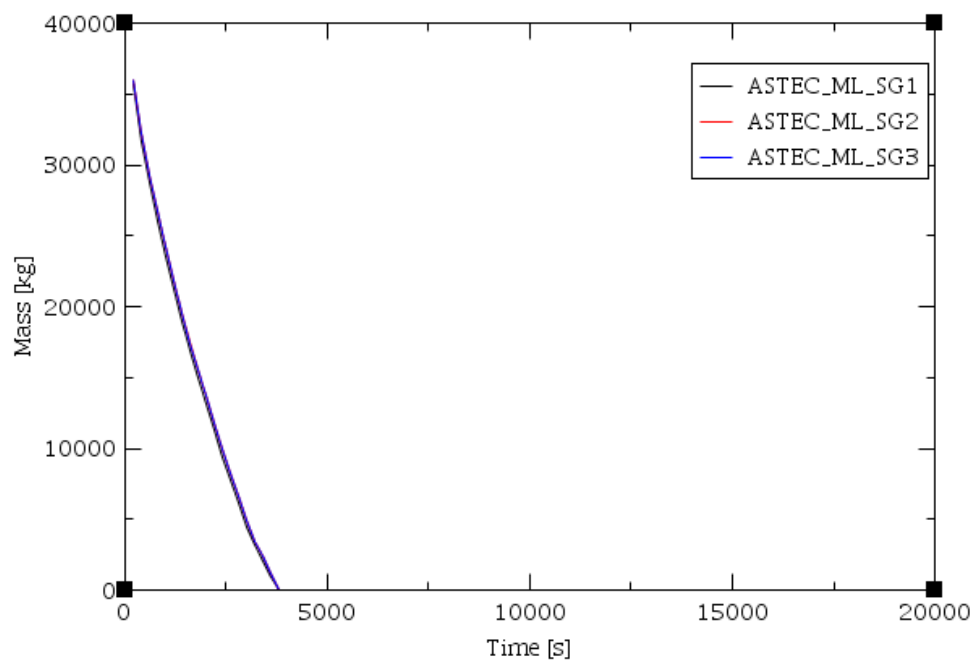
Figure 5-11   SG1/2/3 Liquid Mass Inventory Versus Time Predicted by ASTEC
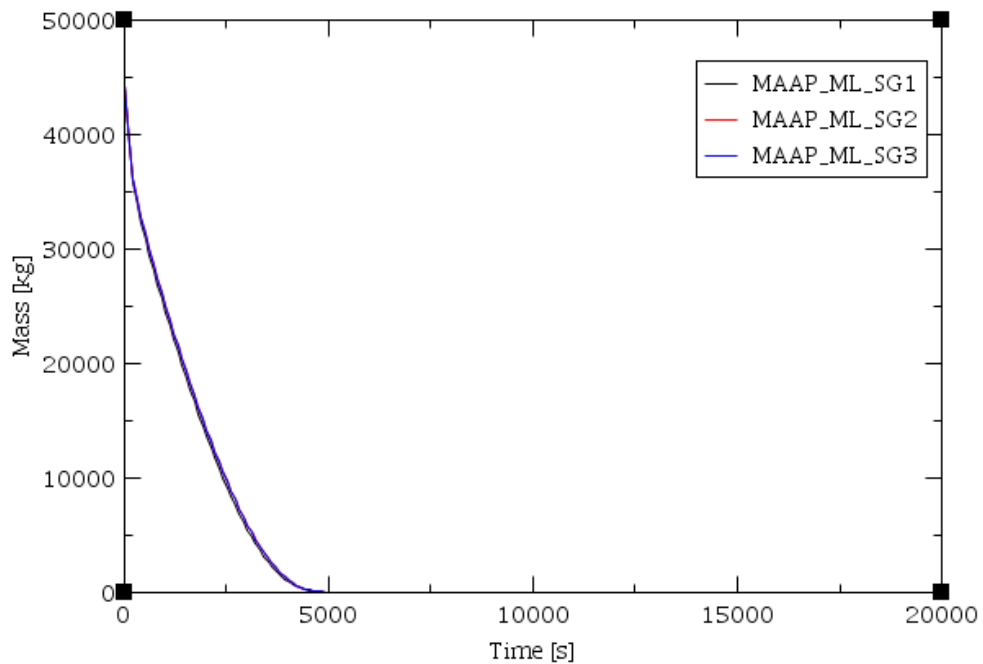
Figure 5-12   SG1/2/3 Liquid Mass Inventory Versus Time Predicted by MAAP
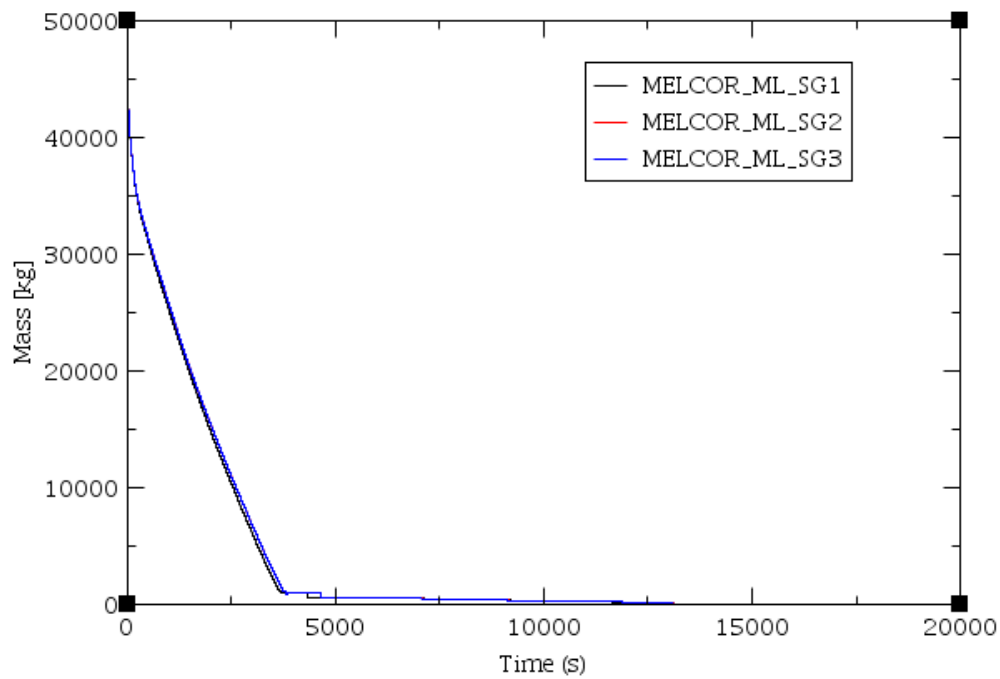
Figure 5-13   SG1/2/3 Liquid Mass Inventory Versus Time Predicted by MELCOR
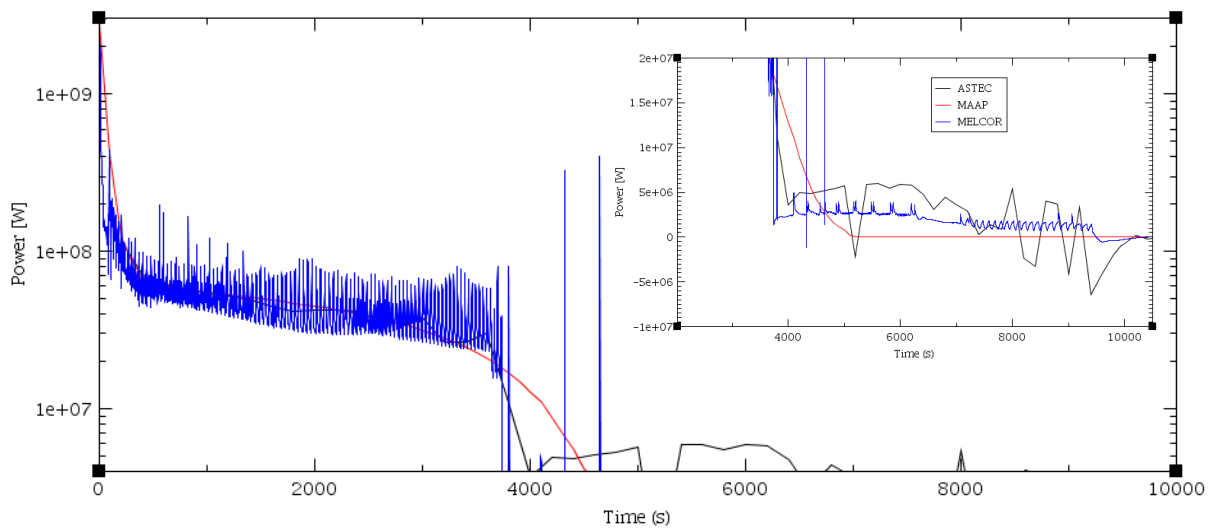
Figure 5-14 Total Heat Transfer Between the Primary to Secondary Side Predicted By ASTEC, MAAP and MELCOR
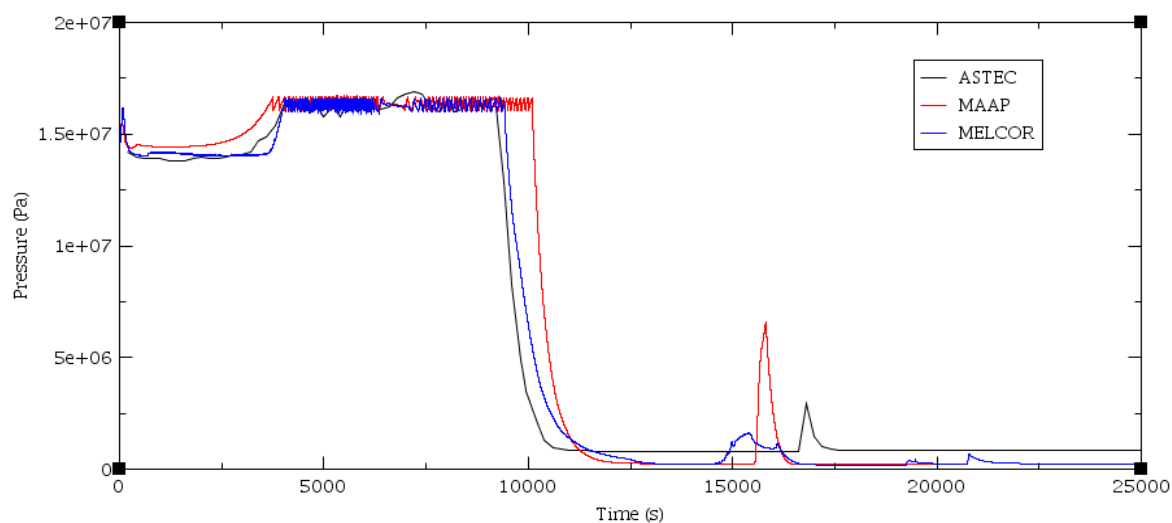
Figure 5-15 Primary Pressure Behavior Versus Time Predicted by ASTEC, MAAP and MELCOR
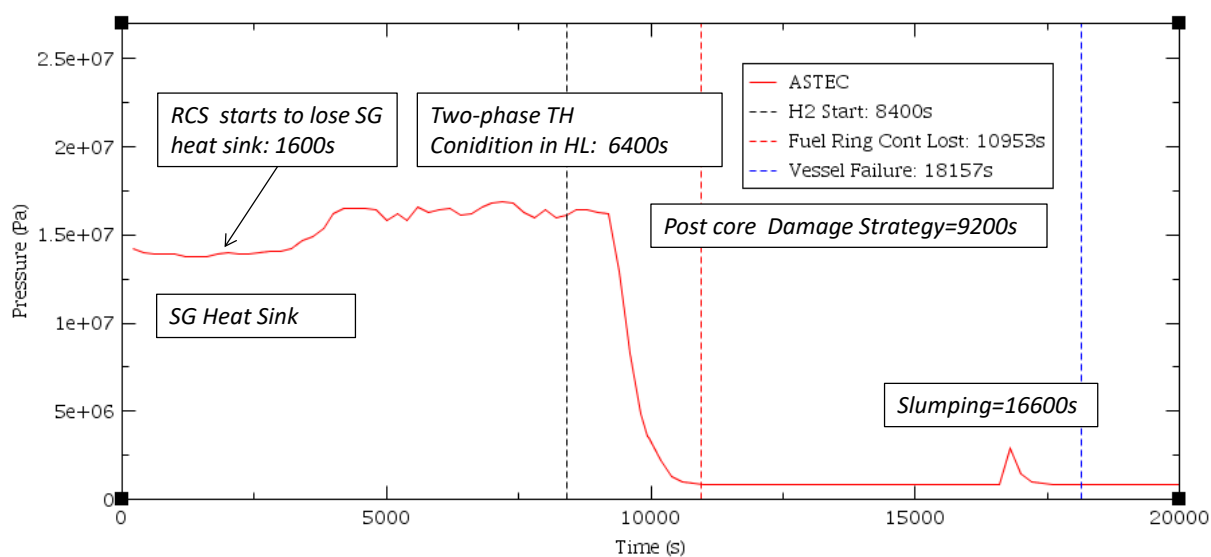
Figure 5-16   Primary Pressure Behavior Versus Time Predicted by ASTEC
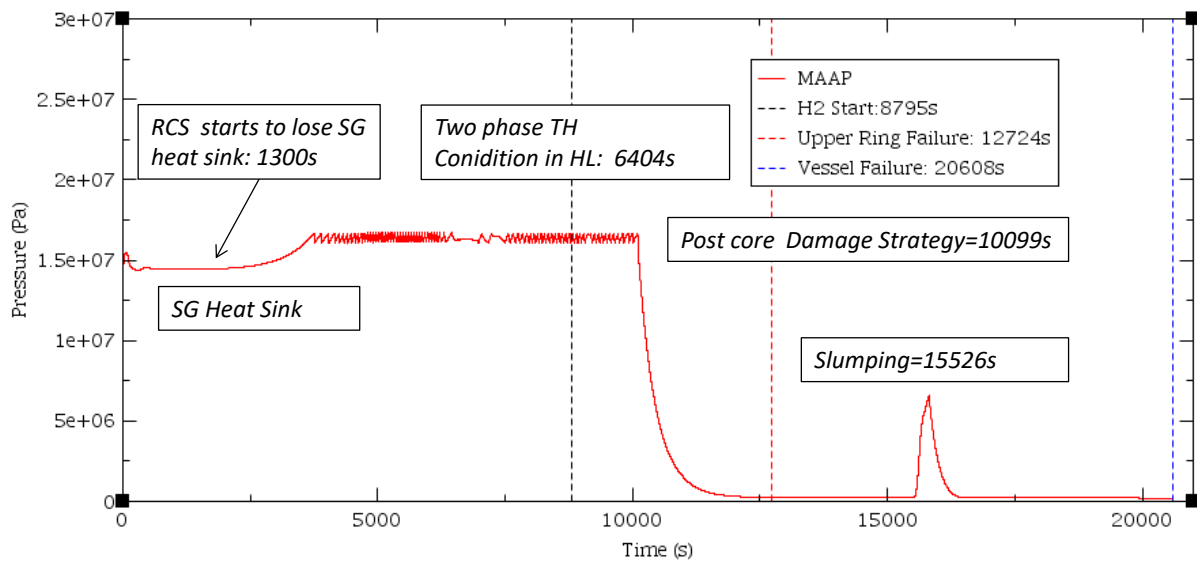
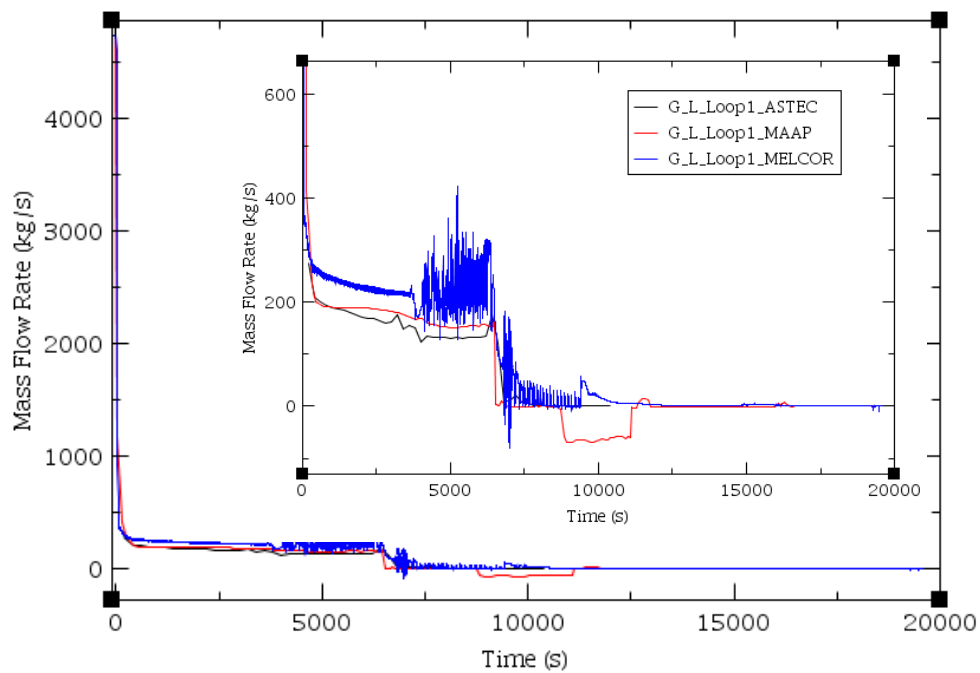**Figure 5-17   Primary Pressure Behavior Versus Time Predicted by MAAP**
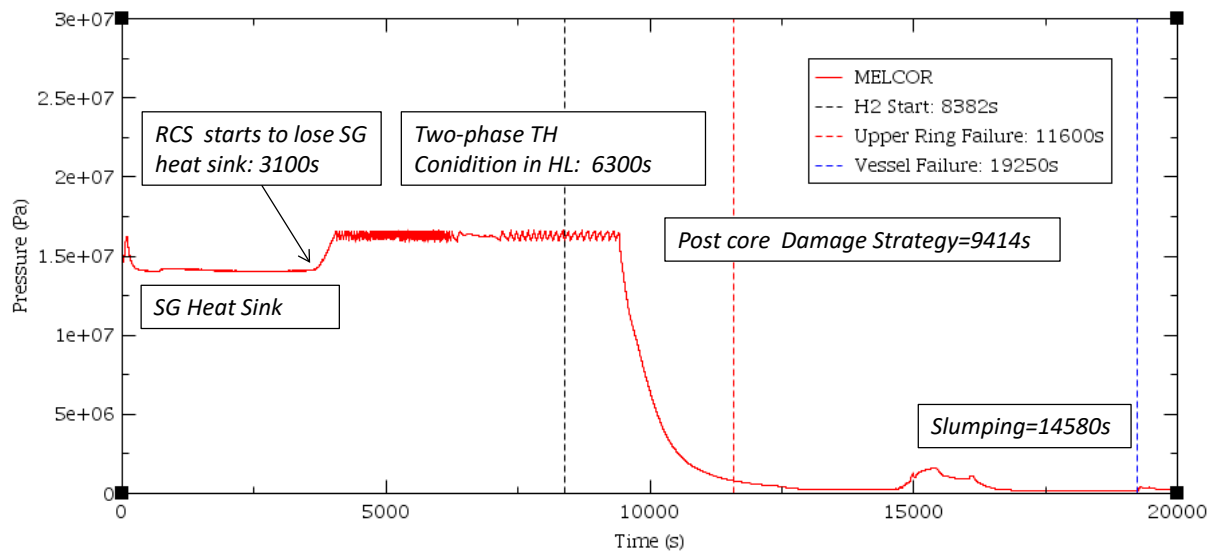
Figure 5-18   Primary Pressure Behavior Versus Time Predicted by MELCOR

Figure 5-19 HL Loop1 Mass Flow Rate Versus Time Predicted by ASTEC, MAAP and MELCOR
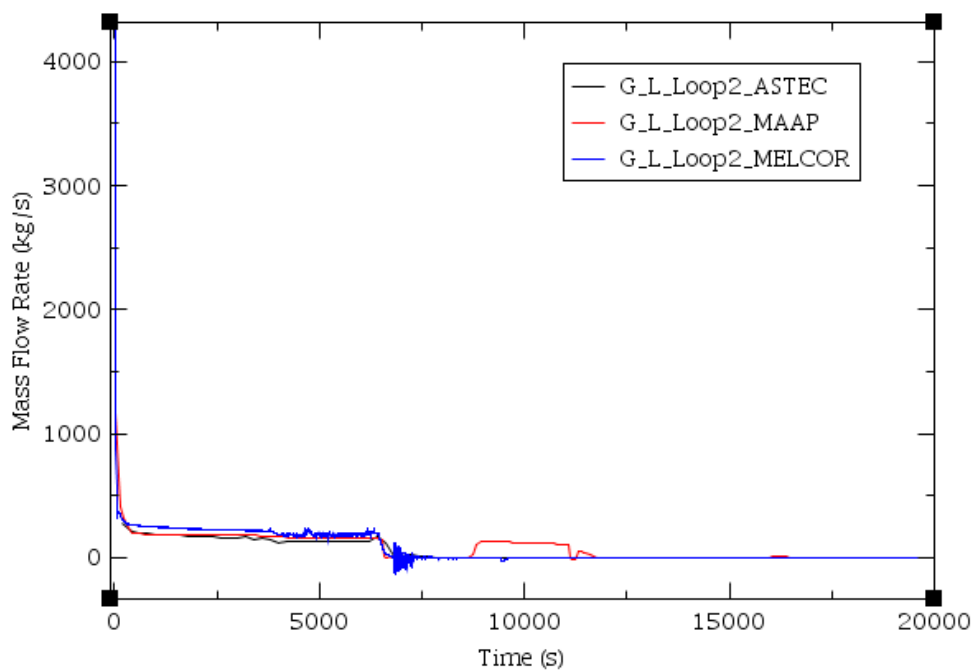

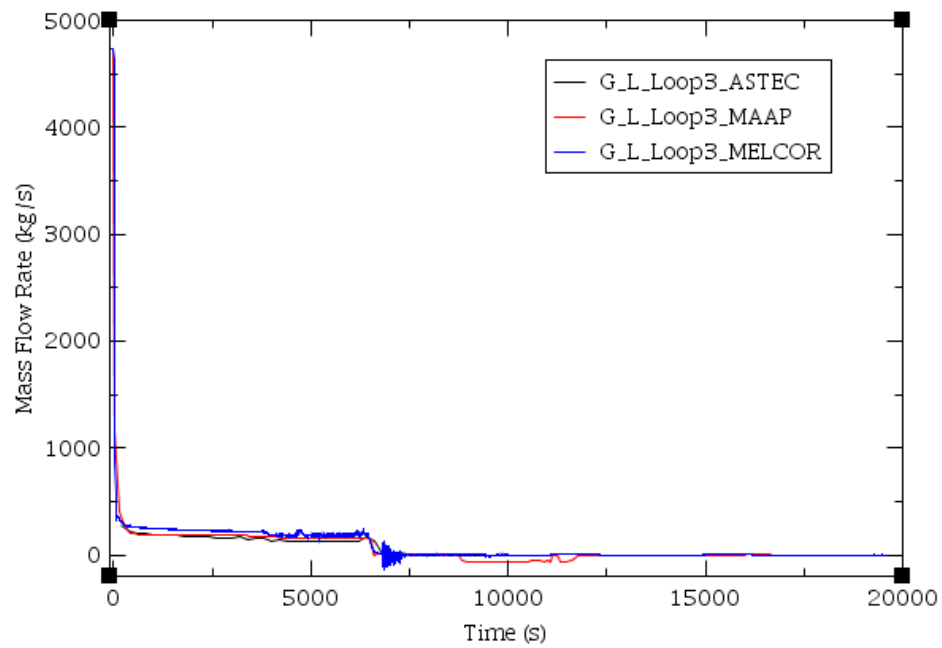**Figure 5-20 HL Loop2 Mass Flow Rate Versus Time Predicted by ASTEC, MAAP and MELCOR**

Figure 5-21 HL Loop3 Mass Flow Rate Versus Time Predicted by ASTEC, MAAP and MELCOR
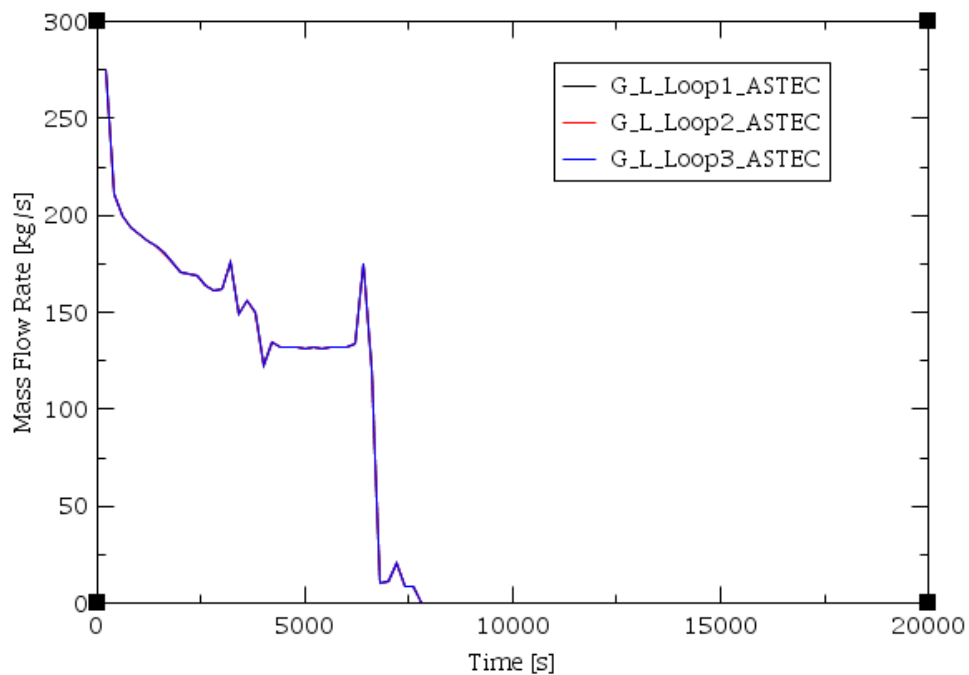

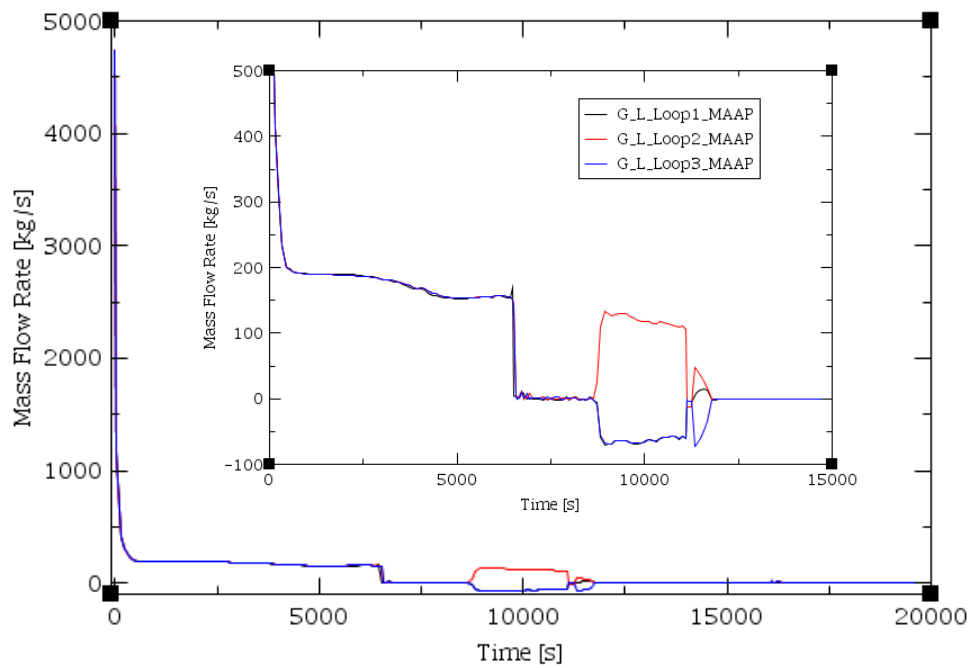**Figure 5-22   ASTEC Loop1/2/3 Liquid Mass Flow Rate Versus Time**

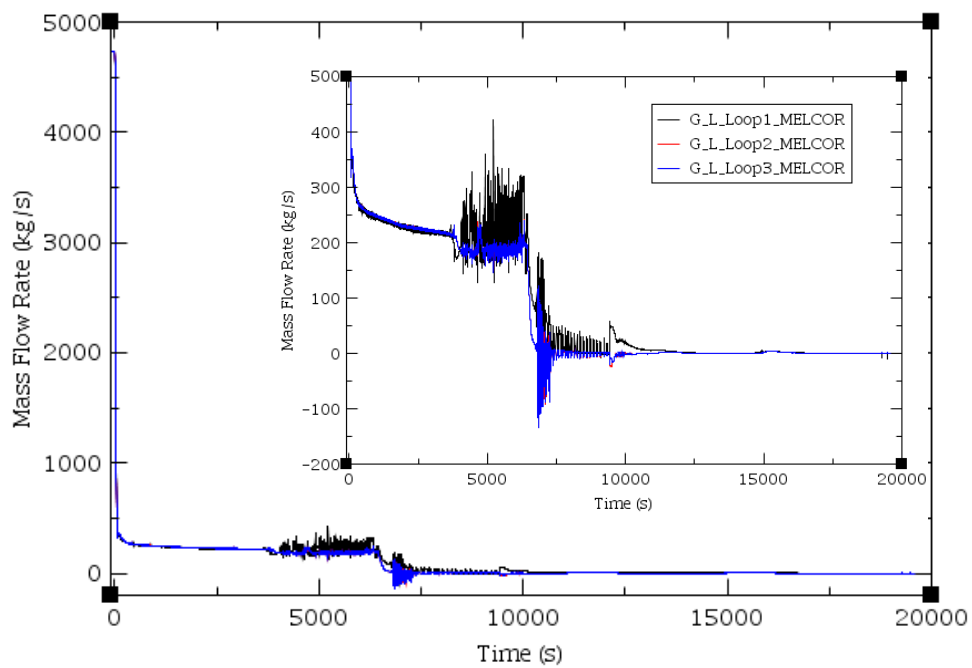**Figure 5-23   MAAP Loop1/2/3 Mass Flow Rate Versus Time**

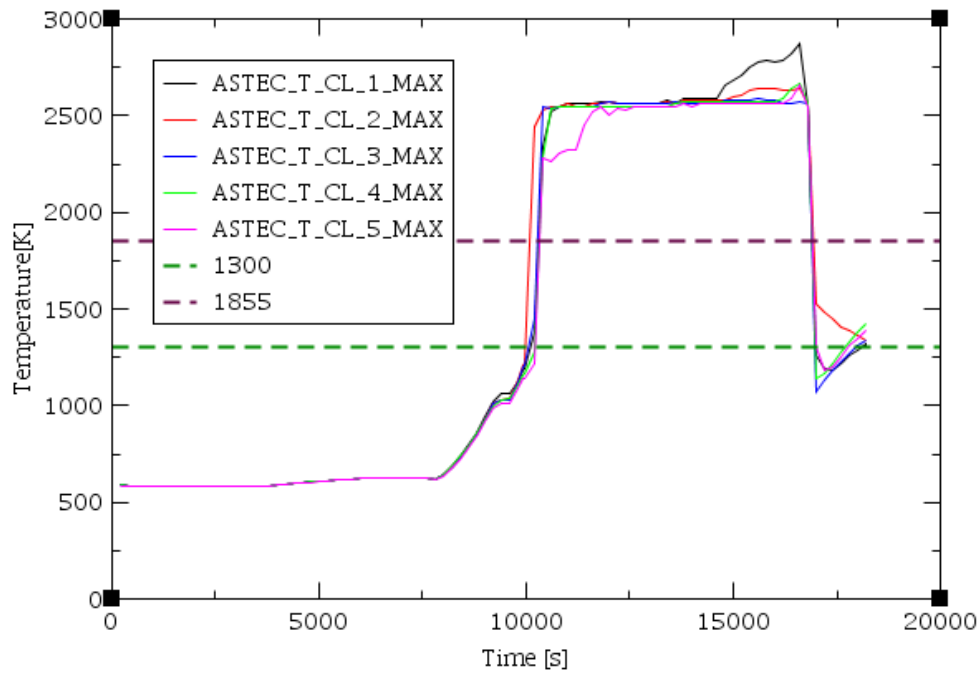**Figure 5-24   MELCOR Loop1/2/3 Mass Flow Rate Versus Time**

Figure 5-25 Max Intact Cladding Temperature at the Different 5 Rings Predicted by ASTEC (maximum value achieved from the beginning of the transient)
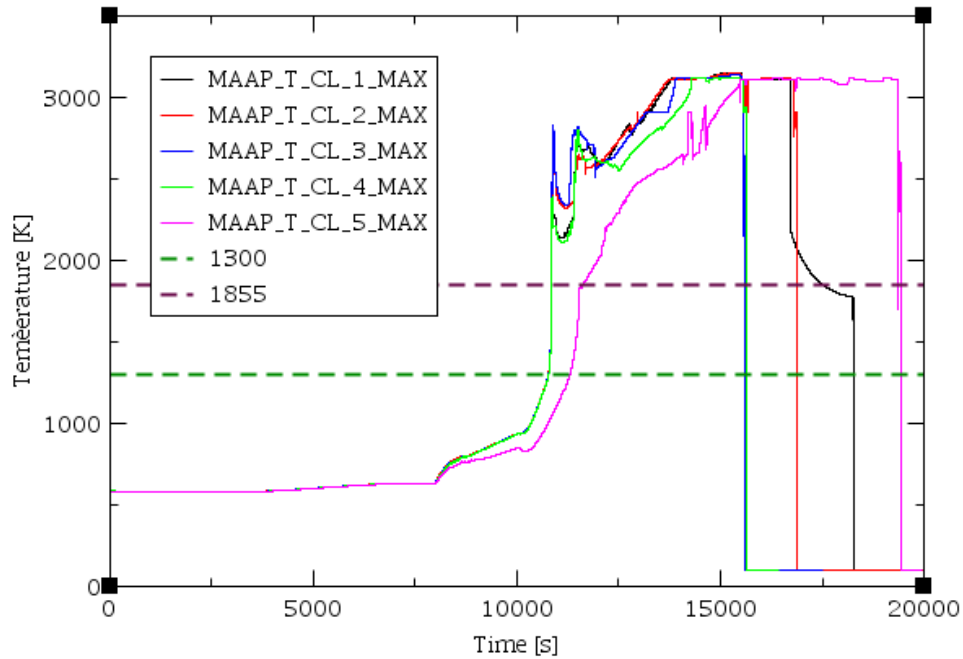

Figure 5-26 Max Intact Cladding Temperature at the Different 5 Rings Predicted MAAP (maximum instantaneous value)
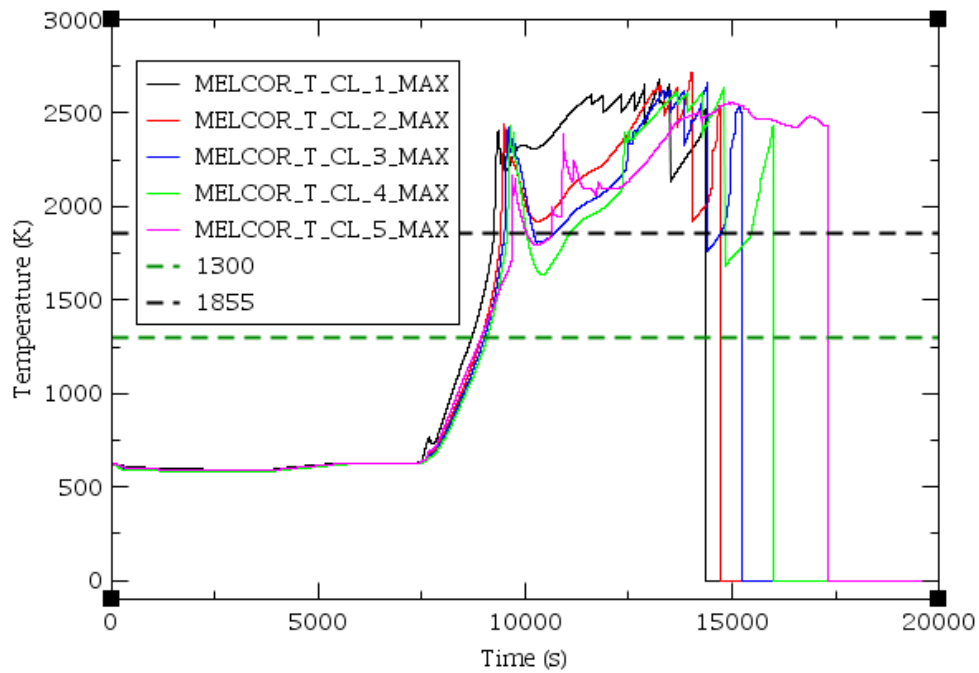
Figure 5-27 Max Intact Cladding Temperature at the Different 5 Rings Predicted by MELCOR (maximum instantaneous value)

Figure 5-28 Max Intact Cladding Temperature Along the 1st Ring Predicted by ASTEC, MAAP and MELCOR

Figure 5-29 Max Intact Cladding Temperature Along the 2nd Ring Predicted by ASTEC, MAAP and MELCOR
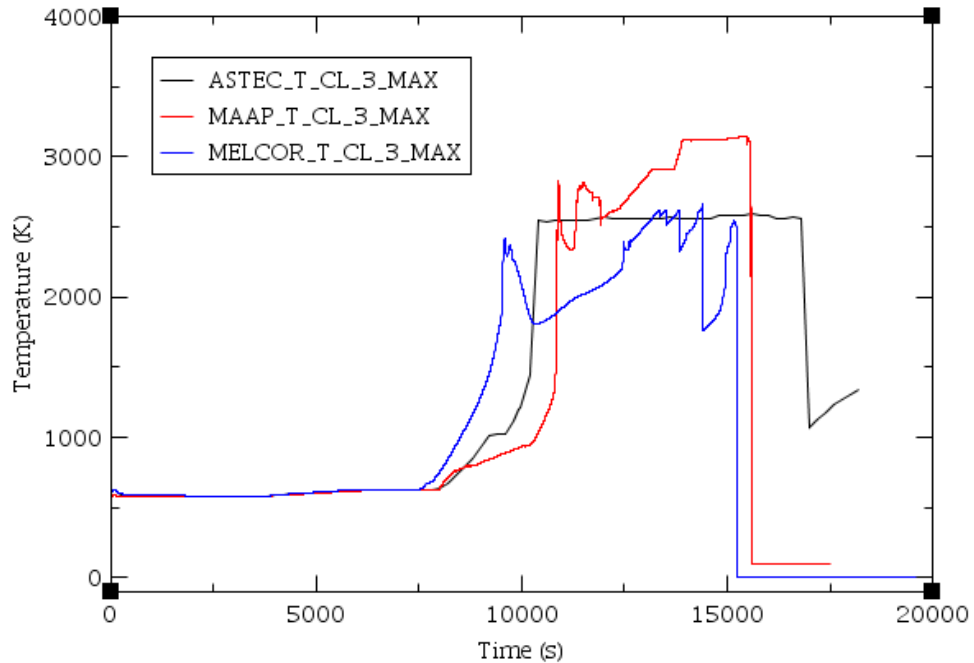
Figure 5-30 Max Intact Cladding Temperature Along the 3rd Ring Predicted by ASTEC, MAAP and MELCOR
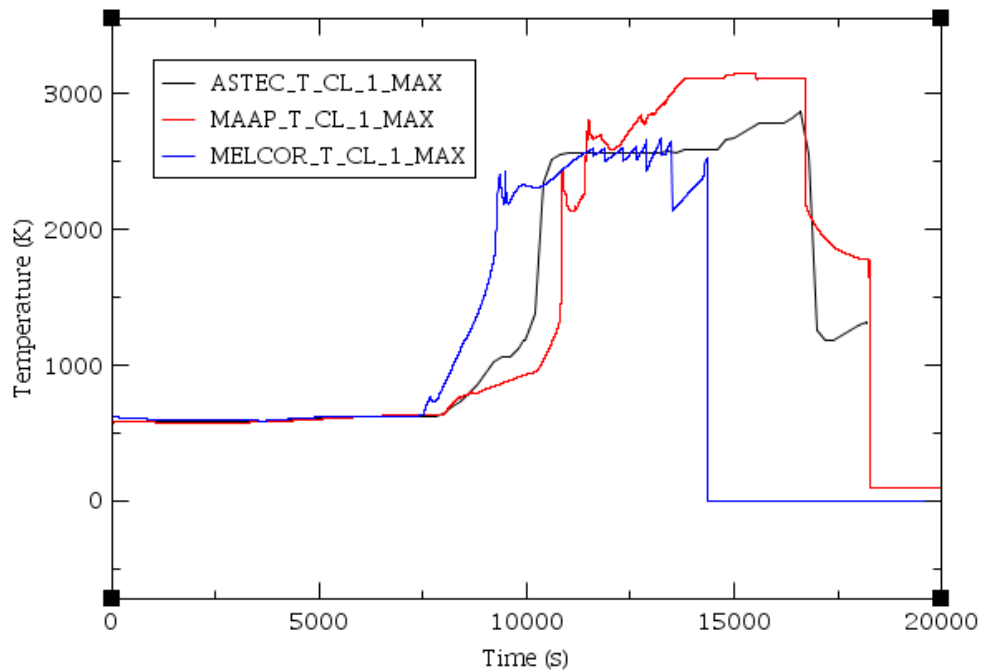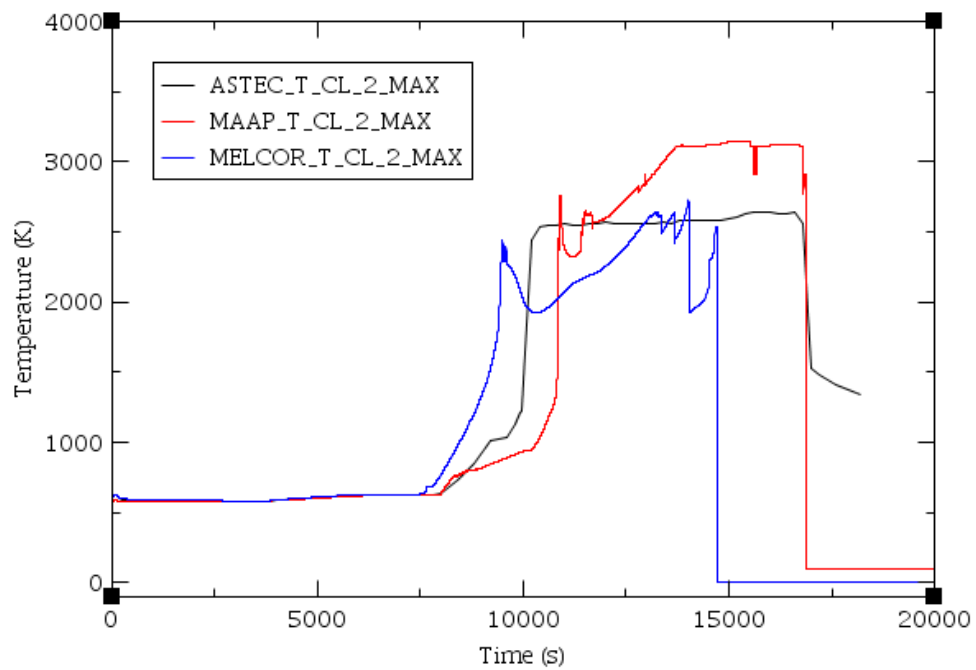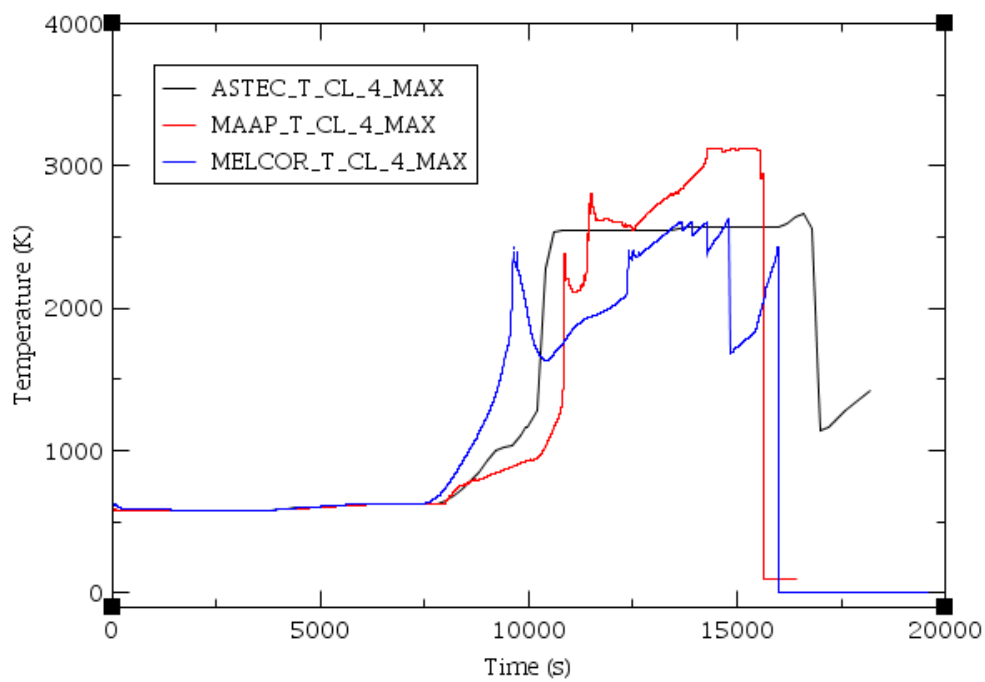
Figure 5-31 Max Intact Cladding Temperature Along the 4th Ring Predicted by ASTEC, MAAP and MELCOR
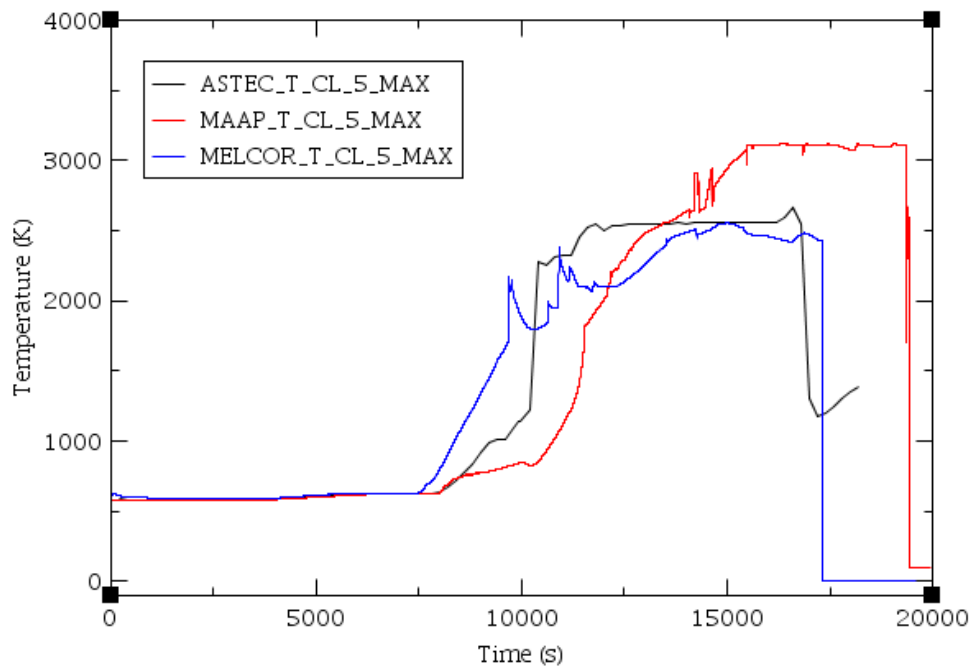
Figure 5-32 Max Intact Cladding Temperature Along the 5th Ring Predicted by ASTEC, MAAP and MELCOR
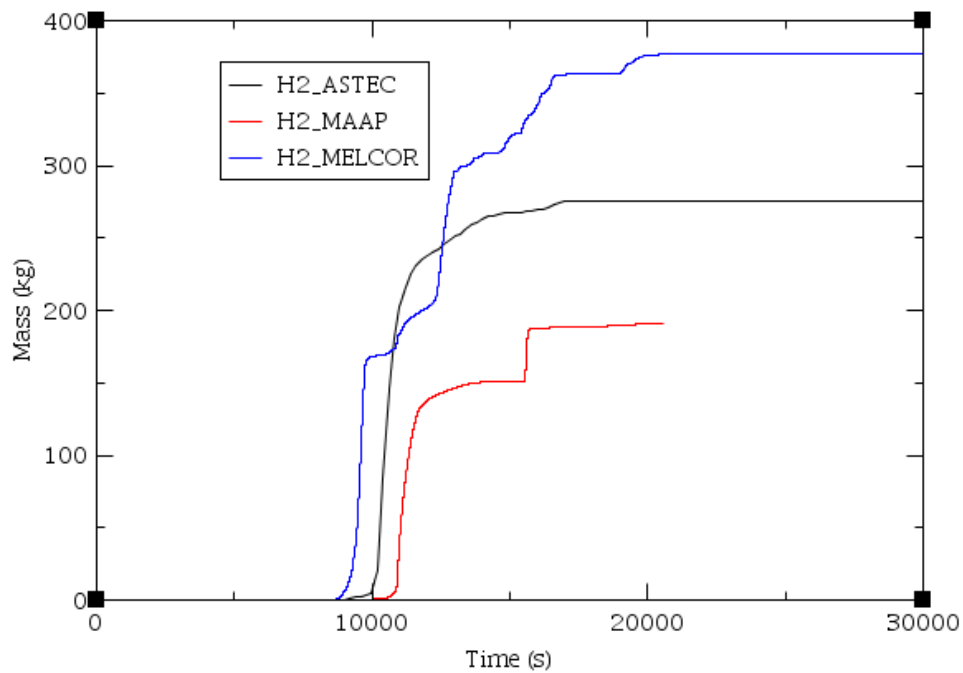
Figure 5-33 Total Hydrogen Generation Versus Time Predicted by ASTEC, MAAP and MELCOR
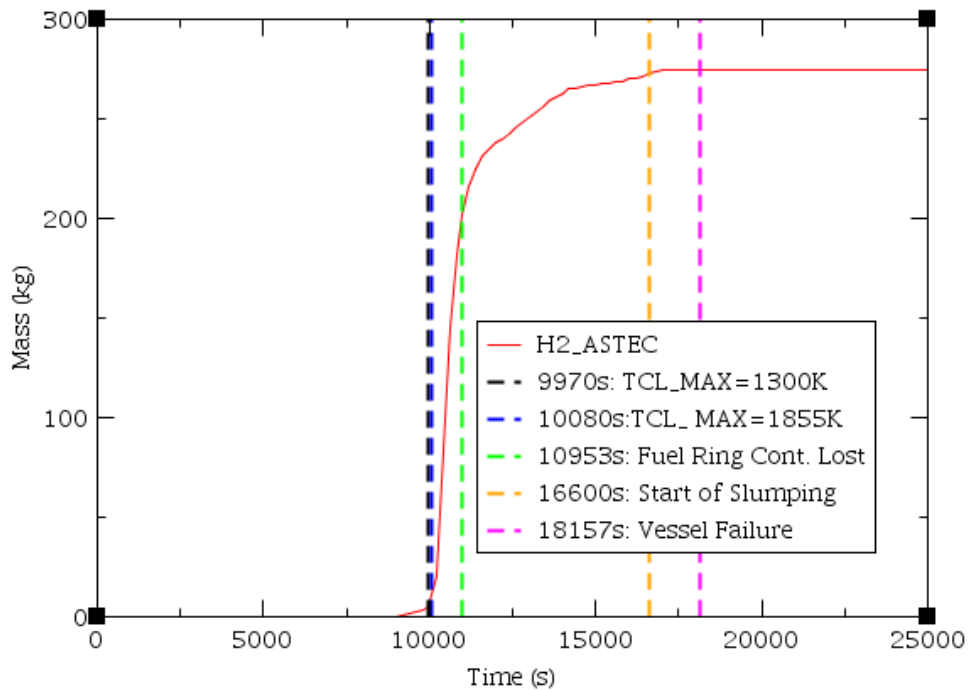
Figure 5-34 Hydrogen Production versus Time Predicted by ASTEC
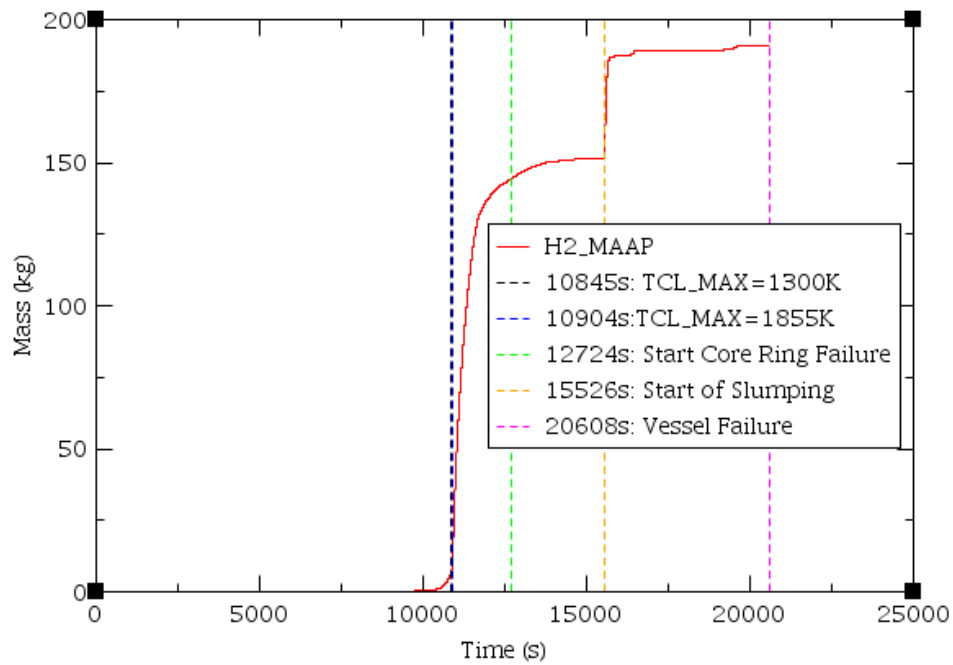
Figure 5-35   Hydrogen Production versus Time Predicted by MAAP
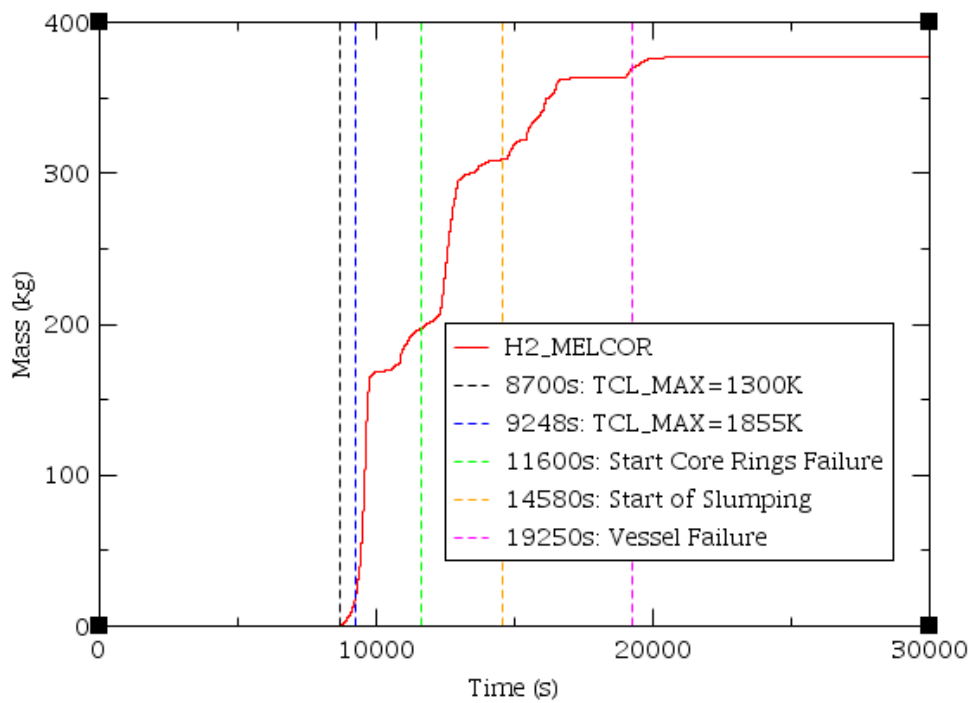
Figure 5-36   Hydrogen Production versus Time Predicted by MELCOR

45
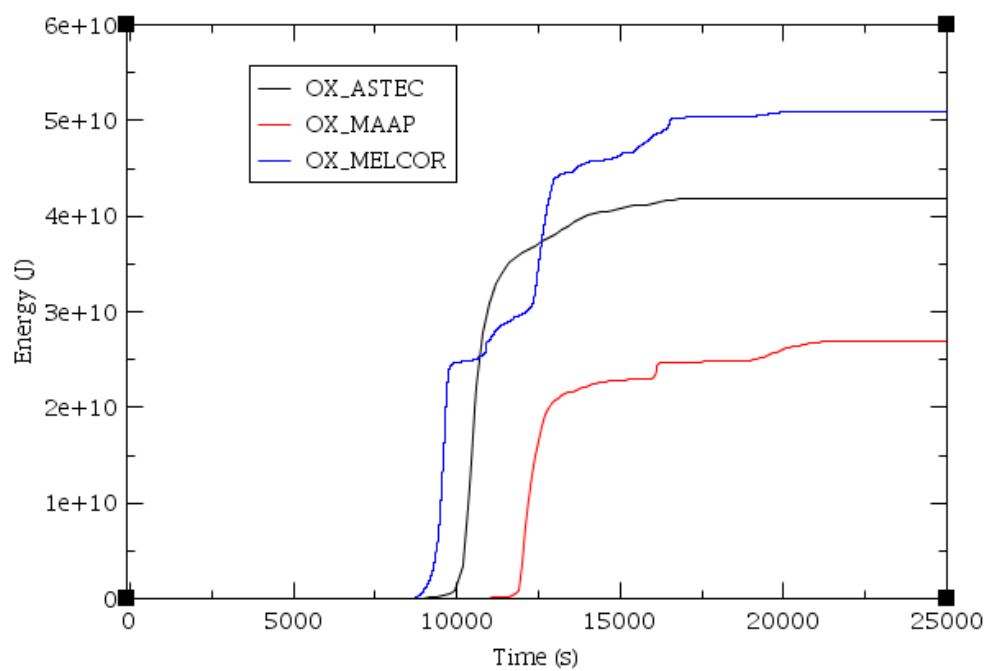
Figure 5-37 Oxidation Energy Generated in the Core versus Time Predicted by ASTEC, MAAP and MELCOR
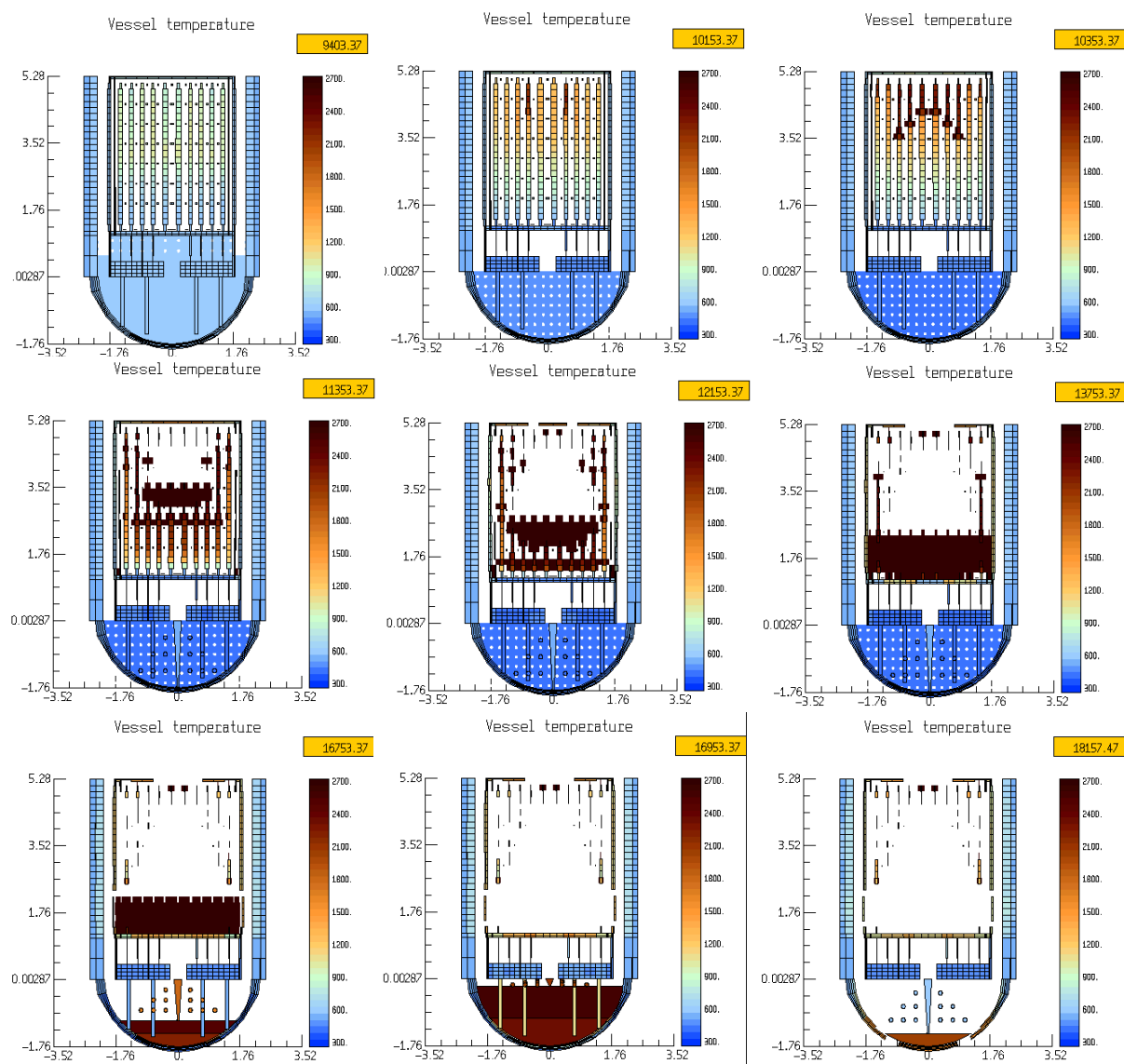
Figure 5-38   ASTEC Core Degradation Representation
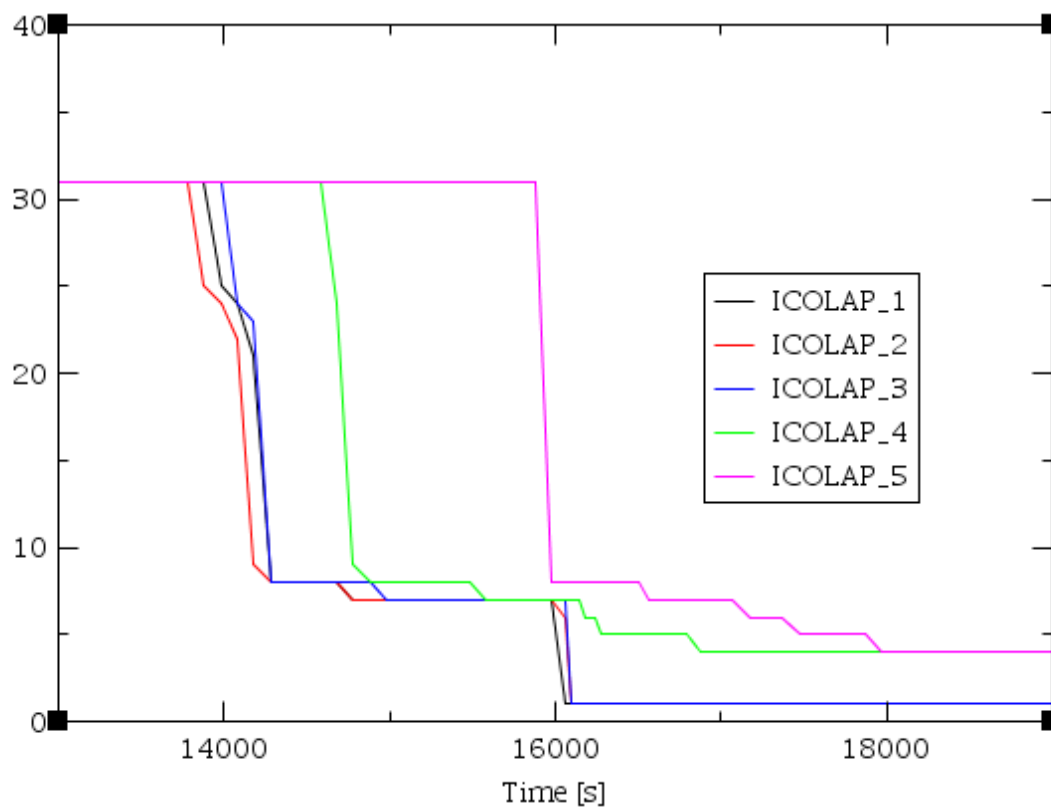
Figure 5-39   Row nº. for Core Collapse in the Channel 1,2,3,4,5 Predicted by MAAP
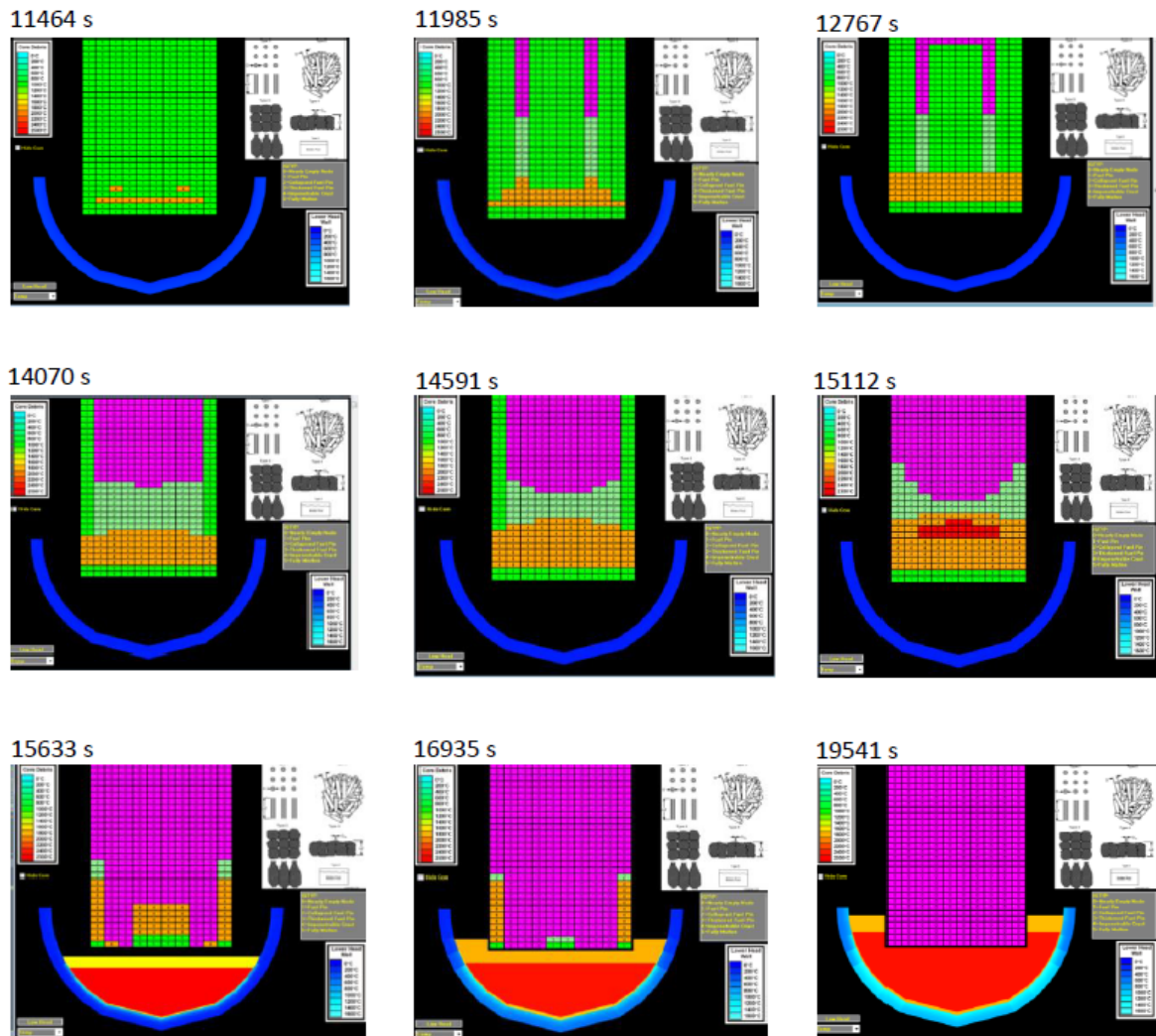
Figure 5-40 MAAP Core Degradation Representation (number 0,1,2,3,4,5 represent the type of degradation that take place in each node; in particular : 0= Nearly Empty Node; 1=Fuel Pin; 2= Collapsed Fuel Pin; 3=Thickened Fuel Pin; 4= Impenetrable Crust; 5= Fully Molten)
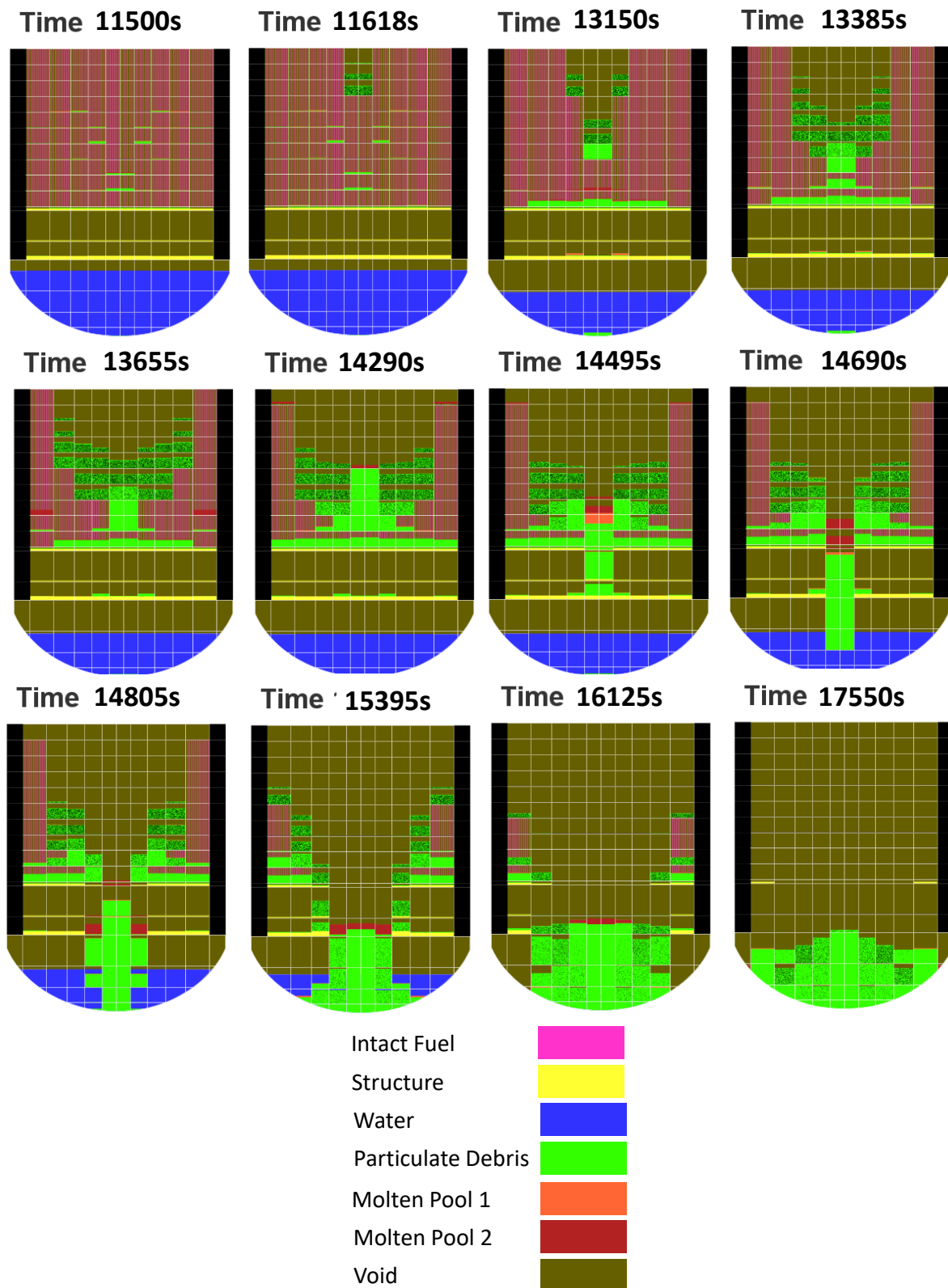
Figure 5-41   MELCOR Code Degradation Phases Representation Made by Using SNAP

6   CONCLUSIONS

The aim of this work, developed in the Code for the European Severe Accident Management (CESAM) project funded in the 7th Framework Programme of the European Commission, is a benchmark exercise to analyze an SBO accident, without any active or passive safety systems, in a 900 MWe, generic Western three-loop PWR design to characterize the main phenomena as a basis for an envisaged accident management strategies evaluation. The analysis of the transient is performed by comparing the results of the best estimate state-of-the-art severe accident codes ASTEC, MAAP and MELCOR. The analysis of the accident evolution is focused mainly on the characterization of main relevant thermal hydraulics and core degradation aspects considering selected main macroscopic safety parameters as a figure of merit (primary pressure, fuel cladding temperature, hydrogen production, inception of the core ring failure, core plate failure, lower head failure) up to the RPV failure. The analysis of the code calculation differences are also presented here to support the phenomenological analyses of the postulated transient.

The results of the calculated data show that the three codes predict the phenomenological evolution in good qualitative agreement with some quantitative differences. Considering the time sequence of relevant phenomenological aspects, the maximum discrepancy between ASTEC and MAAP/MELCOR is about 20% for the main selected safety related parameters used as the figure of merit. The most relevant differences are observed in the in-vessel hydrogen mass production prediction. Such discrepancies underline some modeling differences between the three codes related to core material degradation/relocation, determining differences in the available area for the oxidation process, different flow blockage conditions, different code node porosity prediction, etc. It is important to note that the area available for the oxidation has a great uncertainty due to the complex phenomena taking place during the degradation and relocation of the core material and the limited full-scale experimental data for validation purpose. There is a phenomenological discrepancy related to the core slumping predictions between ASTEC and MAAP/MELCOR calculations. While MAAP and MELCOR predict a core lower plate failure with a consequent relocation of degraded core material in the lower plenum, ASTEC predicts the relocation of the degraded core material through the shroud failure. In the ASTEC calculation hydrogen is produced before the core relocation in the lower plenum, while in the MAAP and MELCOR calculations some further hydrogen is also produced during this phase.

Considering the hypotheses of the transient (no ECCS intervention, scram at zero, no pump leakage, etc.) and the maximum degree of freedom left to the code user (hydraulic and core nodalization strategy and degree of detail, and setting of the boundary conditions) and the general phenomenological agreement of the transient phenomenology predicted by the three codes (with the exception of the slumping phenomenology) the results of the code calculations can be used as a confirmation of the transient phenomenological evolution of the postulated accident. Some secondary phenomenological discrepancies between the code results (i.e. secondary pressure asymmetric behavior between the loops when the secondary side is empty of liquid, different secondary and primary side valve cycling frequency, asymmetric loop behavior during hot steam natural circulation phase) are considered of secondary importance in relation to the selected figures of merit. However, it is important to note that some of these discrepancies could have an effect if other figures of merit are considered. For example, the effect of the asymmetric loop behavior during the hot steam natural circulation should be investigated because it could have an influence for the distribution of the core energy in the

RPV confining structures and the consequent thermal induced degradation phenomena. Therefore, more comprehensive analysis is suggested to investigate these phenomena.

A detailed quantitative analysis of the core energy balance (decay energy in the core, oxidation energy, stored energy in the core, radiative heat loss, convective heat loss), core degradation and relocation, corium physical and chemical composition together with the influence played by natural circulation flows between the core, upper plenum and SGs predicted by the three codes is not presented here but planned for further research. This activity, in collaboration with the code developers could be the basis for a future PWR "crosswalk activity" to investigate the code calculated differences through the identification of the principal modelling capability of each code and the user effect. Future activities should focus on analysis between core structure nodalizations (geometry and mass).

7 REFERENCES

[1] *Severe Accident Management Programmes for Nuclear Power Plants*, IAEA Safety Standards, Safety Guide No. NS-G-2.15, IAEA, Vienna, 2009.

[2] A. Bentaïb, H. Bonneville, G. Cénérino, B. Clément, F. Corenwinder, M. Cranga, G. Ducros, F. Fichot, D. Jacquemain, C. Journeau, V. Koundy, D. Leteinturier, D. Magallon, R. Meignen, F. Monroig, G. Nahas, F. Pichereau, E. Raimond, J-M. Seiler, B. Tourniaire, J-P. Van-Dorsselaere; D. Jacquemain, Coordinator; *Nuclear Power Reactor Core Melt Accidents, Current State of Knowledge,* IRSN, EDP Sciences, France, 2015.

[3] M. Pescarini, F. Mascari, D. Mostacci, F. De Rosa, C. Lombardo, F. Giannetti, *Analysis of Unmitigated Large Break Loss of Coolant Accidents using MELCOR Code*, 35th UIT Heat Transfer Conference (UIT2017), IOP Conf. Series: Journal of Physics: Conf. Series 923 (2017) 012009.

[4] F. Mascari, J. C. De LA Rosa Blul, M. Sangiorgi, G. Bandini, *ASTEC, MAAP and MELCOR Benchmark Code Analysis of an Unmitigated SBO Transient in a PWR-900 Like Reactor*, Proceedings of IAEA Technical Meeting on the Status and Evaluation of Severe Accident Simulation Codes for Water Cooled Reactors, October 2017,

[5] F. Mascari, M. Donorio, F. Giannetti, G. Caruso, A. Naviglio, *Analisi di Transitori non Mitigati: Perdita di Refrigerante da Piccola Rottura in PWR, Perdita D'acqua di Alimento del GV in PWR e SBO in BWR* ADPFISS-LP1- 103, Italy, 2017. http://openarchive.enea.it/handle/10840/9211

[6] F. Mascari, Marco Pescarini, F. Giannetti, I. Luciani, G. Caruso*, Integral Calculations of Severe Accident Scenarios in PWRs and BWRs*, ADPFISS-LP1-075, Italy, 2016. http://openarchive.enea.it/bitstream/handle/10840/8170/ADPFISS-LP1-075.pdf?sequence=1

[7] C. Lombardo, F. Mascari, P. Buffa, F. Castiglia, M Giardina, G. Palermo, *Nodalizzazione MELCOR per lo Studio Integrale di Sequenze Incidentali su Reattori PWR da 900 Mwe e Valutazioni Preliminari D'impatto a Breve e Medio Raggio* ADPFISS-LP1-026, Italy, 2014. http://openarchive.enea.it/bitstream/handle/10840/4957/ADPFISS-LP1-026%20.pdf?sequence=1

[8] P. Chatelard, S. Belon, L. Bosland, L. Carénini, O. Coindreau, F. Cousin, C. Marchetto, H. Nowack, L. Piar, L. Chailan, *Main Modelling Features of ASTEC V2.1 Major Version*, Annals of Nuclear Energy, Vol. 93, July 2016, Pages 83-93.

[9] Http://www.irsn.fr/EN/Research/Scientific-tools/Computer-codes/Pages/The-ASTEC-Software-Package-2949.aspx

[10] Fauske & Associates, LLC *"Transmittal Document for MAAP5 Code Revision MAAP 5.02"*, FAI/13-0801, 2013.

[11] Http://www.fauske.com/nuclear/maap-modular-accident-analysis-program

[12]   *MELCOR Computer Code Manuals*, Vol.1: Primer and Users' Guide, SAND
          2015-6691 R; Vol. 2: *Reference Manual*, SAND 2015-6692 R; Vol. 3: *MELCOR
          Assessment Problems,* SAND 2015-6693 R; Sandia National Laboratories, USA, 2015.

[13]   Http://melcor.sandia.gov/

[14]   J.P. Van Dorsselaere, M. Barrachin, S. Power, M. Adorni, M. Hrehor, F. Mascari, A.
          Schaffrath, I. Tiselj, E. Uspuras, Y. Yamamoto, D. Gumenyuk, N. Fedotova, O. Cronvall,
          P. Liska, *ETSON Strategic Orientations on Research Activities: ETSON Research Group
          Activity*, ATW-International Journal for Nuclear Power, Vol. 63, 2018, issue 1, January.

[15]   *Source Term Uncertainty, Recent Development in Understanding Fission Product
          Behaviour*, NEA/CSNI/R(92)2, Committee on the Safety of Nuclear Installations OECD
          Nuclear Energy Agency, France, 1992.

[16]   *SOAR on Containment Thermalhydraulics and Hydrogen Distribution*,
          NEA/CSNI/R(1999)16, Prepared by an OECD/NEA Group of Experts, June 1999.

[17]   *In-Vessel Core Degradation Code Validation Matrix*, Update 1996-1999,
          NEA/CSNI/R(2000)21, OECD Nuclear Energy Agency, France, 2001.

[18]   *State-Of-The-Art Report on Nuclear Aerosols*, NEA/CSNI/R(2009)5, Organisation for
          Economic Co-operation and Development, Nuclear Energy Agency Committee on The
          Safety of Nuclear Installation, 2009.

[19]   *Containment Code Validation Matrix*, NEA/CSNI/R(2014)3, Organisation for Economic
          Co-operation and Development, Nuclear Energy Agency Committee on The Safety of
          Nuclear Installation, 2014.

[20]   F. Mascari, H. Nakamura, K. Ummlnger, F. De Rosa, F. D'Auria, *Scaling Issues for the
          Experimental Characterization of Reactor Coolant System in Integral Test Facilities and
          Role of System Code as Extrapolation Tool*, Proceeding of International Topical Meeting
          on Nuclear Reactor Thermal Hydraulics 2015, NURETH 2015, Vol. 6, 2015, Pages
          4921-4934.

[21]   J. P. Van Dorsselaere, J. Mustoe, S. Power, M. Adorni, A. Schaffrath, A. Nieminen,
          *ETSON Views on R&D Priorities for Implementation of the 2014 Euratom Directive on
          Safety of Nuclear Installations*, Kerntechnik: Vol. 81, Issue 5, 2016, Pages 527-534.

[22]   L. Humphries, *MELCOR Code Development Status EMUG 2018*, 10th Meeting of the
          European MELCOR User Group, University of Zagreb, Zagreb, Croatia, Faculty of
          Electrical Engineering and Computing – FER, April 25-27, 2018.
          https://www.psi.ch/emug/Emug2018EN/EMUG_2018_01.pdf

[23]   *Modular Accident Analysis Program (MAAP) - MELCOR Crosswalk, Phase 1 – Study*.
          EPRI, Palo Alto, CA: 2014. 3002004449.

[24]   D. L. Luxat, D. A. Kalanich, J. T. Hanophy, R. O. Gauntt, R. M. Wachowiak, *MAAP-
          MELCOR Crosswalk Phase 1 Study*, Nuclear Technology, Vol. 196, Issue 3, 2016,
          Pages 684-697.

[25]   S. Belon, C. Bouillet, H. Bonneville, N. Andrews, C. Faucett, *Insight of Core Degradation Simulation in Integral Codes throughout ASTEC/MELCOR Crosswalk Comparisons and ASTEC Sensitivity Studies*, Proceedings of the 8th European Review Meeting on Severe Accident Research ERMSAR-2017, Warsaw, Poland, May 16-18, 2017.

[26]   *Good Practices for User Effect Reduction, Status Report*, NEA/CSNI/R(98)22, Organisation for Economic Co-operation and Development, Nuclear Energy Agency Committee on The Safety of Nuclear Installation, 1998.

[27]   *Approaches and Tools for Severe Accident Analysis for Nuclear Power Plants*, IAEA Safety Reports Series No. 56, IAEA, Vienna, 2008.

[28]   CESAM, D40.44 – *Synthesis of Evaluation of the Impact of SAM Actions Through ASTEC NPP Calculations*, 2017.

[29]   F. Mascari, J.C. De La Rosa Blul, M. Sangiorgi, G. Bandini, *Analyses of an Unmitigated Station Blackout Transient with ASTEC, MAAP and MELCOR Codes*, SICNUC – PC28 – 001, Italy, 2017.

[30]   F. Mascari, J.C. De La Rosa Blul, M. Sangiorgi, G. Bandini, *Analyses of an Unmitigated Station Blackout Transient with ASTEC, MAAP and MELCOR Code*, 9th Meeting of the European MELCOR User Group, Madrid, Spain, April 6-7, 2017.

[31]   *SCDAP/RELAP5 Thermal-hydraulic Evaluations of the Potential for Containment Bypass During Extended Station Blackout Severe Accident Sequences in a Westinghouse Four-Loop PWR*, NUREG/CR-6995, 2010.

[32]   H. Nowack, P. Chatelard, L. Chailan, St. Hermsmeyer, V. Sanchez, L. Herranz, *CESAM – Code for European Severe Accident Management, EURATOM Project on ASTEC Improvement*, Annals of Nuclear Energy, Vol. 116, June 2018, Pages 128-136.

[33]   L. Foucher, *ASTEC V20R3 PWR900 Like ASTEC Input Deck*, Rapport n° PSN-RES/SAG/2013-451.

[34]   L. Foucher, ASTEC V20R3, *PWR900 Like ASTEC Steady State Calculation*, Rapport n° PSN-RES/SAG/2013-466.

[35]   *SARNET: Network of Excellence for a Sustainable Integration of European Research on Severe Accident Phenomenology and Management – Phase 2*, 2008. EC 7th Framework Programme, April 2008.

[36]   J.-P. Van Dorsselaere, A. Auvinen, D. Beraha, P. Chatelard, C. Journeau, I. Kljenak, A. Miassoedov, S. Paci, Th.W. Tromm, R. Zeyen, *Some Outcomes of the SARNET Network on Severe Accidents at Mid-term of the FP7 project.* Proceedings of the International Conference on Advances in Nuclear Power Plants - ICAPP-2011, Nice, France, May 2–5.

[37]   J.-P. Van Dorsselaere, A. Auvinen, D. Beraha, P. Chatelard, L.E. Herranz, C. Journeau, W. Klein-Hessling, I. Kljenak, A. Miassoedov, S. Paci, R. Zeyen, *Recent Severe*

Accidents Research: Synthesis of the Major Outcomes from the SARNET Network, Nuclear Engineering and Design, Vol. 291, 2015, Pages 19–34.

[38]   *MELCOR Best Practices as Applied in the State-of-the-Art Reactor Consequence Analyses (SOARCA) Project*, NUREG/CR-7008, August 2014.

[39]   *Symbolic Nuclear Analysis Package (SNAP)*, 2007. User's Manual. Applied Programming Technology, Inc. Bloomsburg, PA.

[40]   *Modular Accident Analysis Program 5 (MAAP5) Applications Guidance: Desktop Reference for Using MAAP5 software-Phase 3 Report* Palo Alto, CA November 2017 (3002010658)

[41]   *State-of-the-Art Reactor Consequence Analysis (SOARCA) Project, Sequoyah Integrated Deterministic and Uncertainty Analyses*, DRAFT REPORT. https://www.nrc.gov/docs/ML1715/ML17156A270.pdf

NRC FORM 335 (12-2010) NRCMD 3.7	U.S. NUCLEAR REGULATORY COMMISSION	1. REPORT NUMBER (Assigned by NRC, Add Vol., Supp., Rev., and Addendum Numbers, if any.)
	BIBLIOGRAPHIC DATA SHEET *(See instructions on the reverse)*	**NUREG/IA-0515**

2. TITLE AND SUBTITLE	3. DATE REPORT PUBLISHED	
	MONTH	YEAR
Analyses of an Unmitigated Station Blackout Transient in a Generic PWR-900 with ASTEC, MAAP and MELCOR Codes	**September**	**2019**
	4. FIN OR GRANT NUMBER	

5. AUTHOR(S)	6. TYPE OF REPORT
F. Mascari (1, J. C. De La Rosa Blul (2, M. Sangiorgi (2, G. Bandini (1	Technical
	7. PERIOD COVERED (Inclusive Dates)

8. PERFORMING ORGANIZATION - NAME AND ADDRESS (If NRC, provide Division, Office or Region, U. S. Nuclear Regulatory Commission, and mailing address; if contractor, provide name and mailing address.)

1) ENEA, Via Martiri di Monte Sole 4, 40129, Bologna, Italy
2) European Commission JRC, Westerduinweg 3, 1755 LE Petten, The Netherlands

9. SPONSORING ORGANIZATION - NAME AND ADDRESS (If NRC, type "Same as above", if contractor, provide NRC Division, Office or Region, U. S. Nuclear Regulatory Commission, and mailing address.)

Division of Systems Analysis
Office of Nuclear Regulatory Research
U.S. Nuclear Regulatory Commission
Washington, D.C. 20555-0001

10. SUPPLEMENTARY NOTES
H. Esmaili, NRC Project Manager

11. ABSTRACT (200 words or less)

The work presented in this report developed by ENEA and European Commission JRC within the Code for European Severe Accident Management (CESAM) project funded by the 7th Framework Programme of the European Commission is focused on the analysis of an unmitigated SBO accident in a generic Western three-loop PWR 900 MWe with MAAP 5.02 and MELCOR 2.1 codes to benchmark ASTEC 2.1 code, in the field of severe accident sequence application, considering selected figures of merit as a basis for comparison until RPV failure. The main thermal-hydraulic and in-vessel core degradation phenomena, as simulated by the three severe accident codes, have been analyzed. A detailed quantitative analysis of the core energy balance, core degradation and relocation, corium physical and chemical composition together with the influence played by natural circulation flows between the core, upper plenum and steam generators predicted by the three codes is not presented here but it is planned for future research activity.

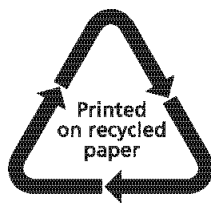| 12. KEY WORDS/DESCRIPTORS (List words or phrases that will assist researchers in locating the report.)	13. AVAILABILITY STATEMENT
Severe Accident, Generic Western Three-loop PWR 900, SBO, ASTEC, MAAP, MELCOR, SNAP, Code to Code Benchmark	unlimited
	14. SECURITY CLASSIFICATION
	(This Page) unclassified
	(This Report) unclassified
	15. NUMBER OF PAGES
	16. PRICE

UNITED STATES
NUCLEAR REGULATORY COMMISSION
WASHINGTON, DC 20555-0001

—————

OFFICIAL BUSINESS

NUREG/IA-0515

Analyses of an Unmitigated Station Blackout Transient in a Generic PWR-900 with ASTEC, MAAP and MELCOR Codes

September 2019